ENSO and its effects on the atmospheric heating processes

Kikuro Miyakoda

Princeton University, USA

Annalisa Cherchi, Antonio Navarra and Simona Masina

Centro Euro-Mediterraneo per i Cambiamenti Climatici, and Istituto Nazionale di Geofisica e Vulcanologia, Bologna, Italy

Jeff Ploshay

Geophysical Fluid Dynamics Laboratory, USA

(Final form for *Journal of Meteorological Society of Japan* on November 2011)

Corresponding author: Annalisa Cherchi, Centro Euromediterraneo per i Cambimaneti Climatici (CMCC),
Viale Aldo Moro 44, 40127 Bologna, Italy.
Tel: +39 051 3782613, Fax: +39 051 3782655, E-mail: annalisa.cherchi@bo.ingv.it

Abstract

El Niño-Southern Oscillation (ENSO) is an important air-sea coupled phenomenon that plays a dominant role in the variability of the tropical regions. Observations, atmospheric and oceanic reanalysis datasets are used to classify ENSO and non-ENSO years to investigate typical features of its periodicity and atmospheric circulation patterns. Among non-ENSO years we have analyzed a group, called type-II years, with very small SST anomalies in summer that tend to weaken the correlation between ENSO and precipitation in the equatorial regions. A unique character of ENSO is studied in terms of the quasi-biennial periodicity of SST and heat content (HC) fields over the Pacific-Indian Oceans. While the SST tends to have higher biennial frequency along the Equator, the HC maximizes it in two centers in the western Pacific sector. The north-western centre, located east of Mindanao, is highly correlated with SST in the NINO3 region. The classification of El Niño and La Niña years, based on NINO3 SST and north-western Pacific HC respectively, has been used to identify and describe temperature and wind patterns over an extended-ENSO region that includes the tropical Pacific and Indian Oceans.

The description of the spatial patterns of the atmospheric ENSO circulation has been extended to tropospheric moisture fields and to low-level moisture divergence during November-December-January, differentiating the role of El Niño when large amounts of condensational heat are concentrated in the central Pacific, from La Niña that tends to mainly redistribute heat to Maritime Continents and higher latitudes. The influence of the described mechanisms on the equatorial convection in the context of the variability of ENSO on longer timescales for the end of the 20^{th} century is questioned. However, the inaccuracy of the atmospheric reanalysis products in terms of precipitation and the shorter time length of more reliable datasets hamper a final conclusion on this issue.

1. Introduction

El Niño is the most powerful large-scale phenomenon in the Northern Hemisphere. In 1980's, the process of El Niño and Southern Oscillation (ENSO) was discussed intensely (for example, Barnett, 1985; Yasunari, 1985; Gutzler and Harrison, 1987), concluding that the anomaly fields of wind and sea surface temperature (SST) evolve in the Indian Ocean and propagate eastward over the Pacific Ocean, culminating in an El Nino event. Besides, it was soon realized that there is a reverse process (La Nina) with cold SST anomalies, tending to propagate westward in the Pacific (McPhaden and Zhang, 2009), and opposite wind anomalies. Recently, Izumo et al., 2010 proposed a mechanism for this propagation from the Indian Ocean to the Pacific, propagation also observed for La Nina events.

The domain of original ENSO region was only the tropical Pacific Ocean (20°N-20°S). See, for example, the summary of Aceituno (1992). However, as seen for example in Barnett (1985), the Pacific and Indian sectors are considered as the connected ocean in terms of the eastward propagation of the atmospheric disturbances. In this respect, it is possible to identify an extended ENSO region that includes the Indian Ocean, and that is larger than the ENSO region defined by Aceituno (1992). The positive and negative ENSO phases are mutually related. And yet the El Nino/La Nina processes do not occur in sequence, but pause periods (non-ENSO) or "benign" periods (Type-II cases) may occur between them, as will be discussed later.

Hunt (1999) stresses that the frequency of El Niño phenomena is essential to consider the variation of climate on the decadal scale. Hansen et al. (1999) have examined the historical record of the temperature at the Earth's surface. The temperature averaged between 23.6ºN and 23.6ºS in their figure (their Fig.7) shows a clear tendency to shift from negative to positive anomalies after 1976. Similarly, the temperature index over the whole globe exhibits an increasing tendency with years.

In this paper, discussion starts with the issue of ENSO in general. Wright (1985), Ju and Slingo (1995) and Wang et al. (2000), for example, pointed out that the timing of ENSO peak is centered on the northern hemisphere winter (NDJ, or DJF), and that anomalous surface winds and SST emerge only in specific years. SST in the eastern Pacific may be influenced by the monsoon convection through the tropical biennial oscillation (TBO; see Meehl, 1987, 1997; Shen and Lau, 1995; Tomita and Yasunari, 1996; Chang and Li, 2000). In particular, the TBO has been identified as the biennial oscillation of the Indian and Australian monsoon rainfall and it is associated with variations in the tropical atmospheric circulation and tropical ocean SSTs (e.g. Meehl, 1987; Lau and Yang, 1996; Chang and Li, 2000; Pillai and Mohankumar, 2008). In general, ENSO emerges over the tropical Pacific Ocean. ENSO variability may have been influenced by the climate shift occurred in 1976. After that, for example, the relationship between ENSO and the Asian Monsoon changed considerably (Kumar et al., 1999; Miyakoda et al., 2000, for example). However, this change on decadal timescale may not be statistically significant (Gershunov et al., 2001).

Webster (1972) and Newell et al. (1972) tried to explain the heating process of the atmosphere-ocean system in terms of condensation. However, their papers were presented too early. Retrospectively it starts to be clear after 1976 that the heat related to water vapor may be linked to increase in SST. One of the issues of this study is to investigate the role of the equatorial convection in the warming trend of the recent decades, and its connection with El Niño events.

The paper is organized as follows. Section 2 describes the main datasets and indices used in the analysis. Section 3 includes the description of the time evolution of El Niño/La Niña events, and the 3-year correlation diagram. Section 4 presents a frequency analysis of the quasi-biennial periodicity. Section 5 describes the atmospheric component of the ENSO oscillation with particular emphasis on the spatial patterns. Section 6 presents the energetics in ENSO events, particularly the precipitation in the equatorial zone. Finally, Section 7

96 contains the main conclusions.

97

98 **2. Datasets and indices**

99 *2.1 Data*

100 The overall approach is to use observations, when available, and re-analysis data.
101 Atmospheric and moisture fields are taken mostly from the ECMWF (European Centre for
102 Medium-Range Weather Forecasts) reanalysis (ERA-40), covering 44 years from 1958 to
103 2001 (Simmons and Gibson, 2000), though it has recently been expanded to include the data
104 from 1957 to 2002 (Andersson et al., 2004; Uppala et al., 2005). SST data come from the
105 HadISST dataset (Rayner et al., 2003). Ocean heat content (HC) data from 1958 to 1999 are
106 taken from an ocean re-analysis product (Masina et al., 2004). The HC is defined as the mean
107 integrated temperature over the first 316 m ocean depth. In this data assimilation, the
108 atmospheric data used for the fluxes at the ocean surface are taken from the NCEP/NCAR
109 reanalysis (Kalnay et al., 1996).

110 Another crucial quantity in this paper is the rate of precipitation. According to Janowiak
111 and Arkin (1991) and Adler et al. (2003), the information of precipitation amount can be
112 derived from satellite observation, *i.e.*, GPCP (Global Precipitation Climatology Project).
113 Therefore, "GPCP climatology is considered a new standard" for the precipitation, though it
114 is only available after 1979. Other datasets of precipitation are used as well. In particular,
115 atmospheric data assimilation outputs coming from the ERA-40 (ECMWF dataset, Uppala et
116 al., 2005), the NCEP-DOE (R-2) (Kanamitsu et al., 2002), and the JRA-25 (Japan
117 Meteorological Agency, 2007) are taken. Actually, ERA-40 seems to include some suspicious
118 components (Kallberg et al., 2005) but it is one of the few datasets covering the period before
119 1979. Another long dataset is the NCEP/NCAR reanalysis (Kalnay et al., 1996) and it has
120 been included in the analysis for completion.

121 *2.2 Indices*

One of the most crucial issues is the selection of El Niño and La Niña events. Following the approaches of Rasmusson and Carpenter (1982), Horel and Wallace (1981) and Trenberth (1997), for example, El Niño years are selected by the values of NINO3 or NINO3.4 SST. The NINO3 index corresponds to the SST averaged in the region 5ºN-5ºS, 150ºW-90ºW, while NINO3.4 region is located at 5ºN-5ºS, 170ºW-120ºW. In this connection, Shukla (1995) and Wang et al. (2000) have found interesting and probably important evidence. The peaks of these phenomena tend to be locked to a particular season, *i.e*., the boreal winter (NDJ). The seasonal phase-locking has been discussed by numerous studies addressing different theories for the ENSO demise (e.g. Harrison and Larkin, 1998; Wang, 2001; Vecchi and Harrison, 2003; Lengaigne et al., 2006), even though Neelin et al., 2000 showed that some El Nino events may have a peak or local maximum in fall or even in the spring season.

In this study to identify El Nino years we used NDJ NINO3 SST from the CDC/NOAA website. In this way, El Niño years treated in this paper are: 1963/64, 65/66, 68/69, 72/73, 76/77, 82/83, 86/87, 87/88, 91/92, and 97/98 (see Table A1) with the season peak at NDJ. For example, NDJ 1963/64 implies that ND(63) and J(64).

Trenberth (1997) states that NINO3.4 SST is most appropriate for determining ENSO. However, Yang et al. (2006) found, based on the sensitivity studies, using the "Breeding" method, that the most sensitive area for perturbation of SST is the region around NINO3, as opposed to NINO3.4. In other words, the selection of NINO3 may be justified by the perturbation theory for a coupled atmosphere-ocean model, even if Yang et al. (2006) results may be strongly model dependent. From an observational point of view, the eastern edge of the warm pool in the central Pacific seems to be the place where the atmospheric response is the strongest (e.g. Palmer and Mansfield, 1984; Kessler et al., 1995; Picaut et al., 1996). However for the selection of El Niño years, NINO3 or NINO3.4 SST, give the same result.

The La Niña years are selected by the values of the NDJ HC (heat content) anomalies in the northwestern lobe (130ºE-170ºE, 2ºN-10ºN) of the Tropical Pacific Ocean. The above

criterion may be partially justified in the framework of the recharge-discharge oscillator theory (Jin, 1997a,b) for ENSO, following the pioneer hypothesis by Wyrtki (1975) that heat content growth in the western Pacific is precursor to ENSO. Actually, the northwestern lobe area defined here is smaller than the western Pacific region considered by Wyrtki (1975) and Jin (1997a,b), however as the correlation coefficient between northwestern lobe NDJ HC and NINO3 NDJ SST is high (-0.78), its usage to identify La Nina years is proper. In fact, as shown in Table 1, La Nina years chosen according to it agree with previous studies classifications. Further, the western lobe here defined is close to NINO6 region (140ºE-160ºE, 8º-16ºN), as defined by Wang (2001) looking for a unified oscillator model for ENSO. The La Niña years we selected are: 1964/65, 67/68, 70/71, 73/74, 75/76, 88/89, 95/96, and 99/00 (see Table A1), with the peak season being NDJ as for El Nino.

Our selections, for both El Nino and La Nina years, mostly agree with previous classifications based on other parameters. For example, Ropelewski and Halpert (1996) classified El Nino and La Nina based on precipitation, and compared to the present study they excluded two cases for El Nino (i.e. 1963/1964 and 1987/1988). Prior to the above, Schneider and Fleer (1989) investigated El Niño based on SST, particularly over the area of 130ºW-80ºW, 0º-5ºS, close to NINO3. Their selection between 1957 and 1985 agrees exactly with the present paper. Harrison and Larkin (1998) and Larkin and Harrison (2002) provided a classification based on SST and wind fields, and their selections exclude one case for La Nina and two cases for El Nino. A summary of the differences between the classification of La Nina years used in the present study and some previous works is shown in Table 1. Overall, the selections mentioned differ by few cases (at least one or two) and according to that the analysis is supposed to be almost invariant.

For the study of the atmospheric issue in the equatorial belt, the amount of rainfall is a good or perhaps best indicator for the dynamics in the tropics. Navarra et al. (1999) extended the concept to use the distribution of rainfall along the tropical belt. TOI (Tropical-wide

Oscillation Index) is defined as the first principal component of the precipitation averaged between 30ºN to 30ºS around the globe, where the "first principal component" is the time series of the first proper-values in the empirical orthogonal function (EOF).

3. ENSO oscillation

3.1 Three types of equatorial SST distribution

Figs. 1a, 1b, 1c show three states of SST distribution over the Pacific-Indian Oceans sector related to La Nina, El Niño and type-II cases, respectively. It evidences that, differently from El Nino and La Nina events, type-II years tend to have smaller anomalies in the region considered. The identification of type-II cases, mostly related to events having small SST amplitudes, is described in Navarra et al. (1999). Further details are given below and summarized in Appendix A.

Fig. 2 shows monthly mean SST anomalies averaged in NINO3 region from January to July organized into two groups: some El Nino and La Nina cases and a number of non-ENSO events (panel a), and the type-II cases classified in table A1 (panel b). Barnett (1991) has shown a similar diagram using surface zonal winds. Fig. 2a indicates that, after the peaks in NDJ, the SST in the east (NINO3 region) decreases rapidly in the boreal spring, in agreement with the climatology. Navarra et al. (1999) identified JAS as the correct season to highlight type-II years in terms of SST anomalies. In fact, the zero-line crossing in spring is common to ENSO and non-ENSO years (fig. 2a), but small values of SST in JAS are typical of the Type-II cases alone (fig. 2b) (see Appendix A for more details on the classification of type-II years).

Many studies have shown the relationship between ENSO and the Tropical Biennial Oscillation (TBO) (*i.e*. Rasmusson and Carpenter, 1983; Yasunari, 1990; Webster and Yang, 1992; Kirtman and Shukla, 2000). For example, Yasunari (1990) shows a lag correlation diagram between the Indian monsoon index, AIR, and the SST in the western equatorial

Pacific (130°E-150°W). The correlation is negative in the previous summer and becomes positive in correspondence of monsoon time and in the months that follow, peaking in winter. In the context of the TBO/ENSO relationship spring is the crucial season for the transition from relatively strong to relatively weak monsoons (e.g. Meehl, 1997).

3.2 The 3-years correlation diagram: All cases

Fig. 3a shows the correlation coefficients between TOI(JAS) and SST monthly anomalies. The x-axis extends from the western Indian Ocean to the eastern Pacific Ocean, thus including the Maritime Continent (MC) sector; the ordinate consists of three years (i.e. Y(-1), Y(0), Y(+1), from top to bottom, where Y(0) corresponds to the year of the JAS average). Hereafter, this type of diagram will be called "the 3-year correlation diagram". It has been already used in literature, i.e. by Lau and Yang (1996) and by Shen and Lau (1995), with the correlation computed between SST and an East Asian Summer Monsoon index. The "3-year correlation diagram" differs from the classical Hovmöeller diagram because the ordinate has only three years (lagged correlations) instead of multiple years. A 3-year representation is chosen as it fits better the ENSO evolution, possibly related with the TBO timescale.

Fig. 3a shows a number of useful information. The domain in x-direction is divided into three parts, *i.e.*, the Indian sector (50ºE-100ºE), the MC-Western Pacific sector (100ºE-160ºE), and the central eastern Pacific sector (160ºE-80ºW). The MC-Western Pacific includes the Maritime Continents region (120°-130°E) and the Western Pacific (warm-pool) region (130°-160°E), whose eastern bound has been identified in previous studies (Picaut et al., 1996; Bosc et al., 2009; Maes et al., 2010). According to the sign of the correlation, the temporal axis is divided into two main parts *i.e*. Apr(-1) – Apr(0) and Apr(0) – Oct (+1) in the Indian sector. Similarly the Pacific sector is divided in two parts, *i.e*., Jan(-1) – Jan (0) and Jan(0) – Jul (+1). The MC-Western Pacific sector is characterized by positive correlations from Apr(0) to Feb (+1) peaking in the late summer. NINO3.4 is located at 170ºW-120ºW, where the correlation coefficient reaches its negative maximum at Oct(0)-Feb(+1).

Fig. 3a permits to evidence the oscillation in the Pacific Ocean. In fact, Pacific SST is positively correlated with TOI(JAS) from Y(-1) to Y(0), and then negatively from Y(0) to Y(+1), consistently with the ENSO period. Y(0) represents a transition for a change in the sign of the correlation not only for the central eastern Pacific sector, but also for the Indian and the MC-Western Pacific sector (fig. 3a).

3.3 The 3-years correlation diagram, excluding type-II cases

By definition, type-II years have weak SST anomalies in JAS and they may influence the relationship between ENSO and the tropical precipitation in summer. To investigate more on that we excluded the type-II cases, defined in table A1, from the entire SST time series and we repeated the correlation obtaining Fig. 3b. That is, the lagged correlation between JAS TOI and monthly SST anomalies is done for all the years in the record except for the ones classified as Type-II, as reported in Table A1. A comparison between the two panels suggests that excluding type-II years the correlation coefficients between JAS TOI and monthly SST increase for the whole domain considered. This result confirms that a quasi-biennial relationship between SST and JAS TOI is strengthened excluding those years that have a weaker signal in summer. In fact, as described in Navarra et al. (1999), the type-II years inhibit the ENSO-monsoon teleconnection in summer.

The similar correlation pattern to Figs. 3a and 3b can be obtained by other indices as well, such as the Southern Oscillation Index (SOI), or Indian Monsoon Index (AIR) (not shown), but the highest correlations are obtained by TOI. Miyakoda et al., (1999) provided an exhaustive investigation of the sensitivity of this analysis to the choice of the tropical index. According to the index chosen, the intensity of the correlation may change but overall the patterns are confirmed. In the Pacific and Indian Oceans, the transition from positive to negative correlations between SST and TOI with respect to Y(0) intensifies in fig. 3b, as the values increase in Oct(0)-Jul(+1). In the Pacific sector, the positive correlation coefficients are intensified during July-October of Y(-1). Lau and Nath (1994) defined the kind of

252 teleconnection described in fig. 3 “the bridging effect”. The bridge is related to an
253 increase/decrease of the Walker circulation and of its ascending branch over the MC.
254 According to that, events like the Indian Ocean Dipole (IOD) and ENSO may co-occur
255 (Murtugudde et al., 2000; Annamalai et al., 2003).
256
257 **4. The quasi-biennial signature**
258 *4.1 The spatial distribution of the quasi-biennial signature*
259 Trenberth (1975) reported the TBO signature in his EOF analysis of the sea-level pressure
260 and SST fields in the Australian area. Since then, the geographical distributions of the
261 biennial periodicity have been presented by a number of authors for SST, surface wind, and
262 precipitation. For example, Ropelewski et al. (1992) showed the connection between the
263 Indian monsoon and the equatorial Pacific process in terms of the surface wind fields.
264 The method of “frequency analysis” by Murakami (1979) is capable of handling this type
265 of problem, as was demonstrated by Tomita and Yasunari (1996). Figs. 4a and 4b display the
266 distributions of quasi-biennial periodicity in SST and HC, respectively, obtained by this
267 method. The reason for the success is as follows. The “wavelet analysis” is suitable for the
268 time series of data that include sharp peak of periodicity, for example, at 24 months. On the
269 other hand, if the time series include broadband periodicities such as 18-36 months together
270 with 12 months, the “frequency analysis” is more suited.
271 Figs. 4a and 4b indicate the percentage (%) at which the anomalies of 18-36 month
272 periods (quasi-biennial period) occupy relative to the total variability of SST and HC,
273 respectively. SSTA and HC data are taken from the ocean analysis by Masina et al. (2004).
274 Fig. 4a is similar to that of Tomita and Yasunari (1996) (their Fig. 7), though crucial
275 differences exist. First, Fig. 4a shows that the most outstanding area of the quasi-biennial
276 periodicity for SST is located along the equator (west of NINO3.4) with the secondary center

277 in the MC. The location of the secondary center is very close to the northern "lobe" in the
278 MC region (east of the Mindanao).

279 The regions with the largest quasi-biennial periodicity in terms of SSTA (fig. 4a)
280 correspond to the location of the key SSTA regions for the identification of the dateline El
281 Nino (Larkin and Harrison, 2005) or of El Nino Modoki (Ashok et al., 2007). The
282 identification of this new type of El Nino follows the finding that toward the end of the 20th
283 century warmer SST anomalies were more common toward the centre of the Pacific Ocean
284 rather than in the east, eventhough a clear explanation of this difference is still missing (Latif
285 et al., 1997; Larkin and Harrison, 2005; Ashok et al., 2007; Kao and Yu, 2009; Kug et al.,
286 2009; Yeh et al., 2009).

287 Now we go one-step further. The map of Tomita and Yasunari (1996) shows the wide
288 spread of quasi-biennial periodicity in South China Sea, the MC, New Guinea, east of
289 Australia (the Arafura Sea), and separately the eastern equatorial Pacific. In our study, the
290 quasi-biennial periodicity centers for SST are located west of NINO3.4, as opposed to
291 NINO3. The maximum is more than 50%. There is another center (45%) near Philippine
292 Island, which is related to the northerly flow at 1000 hPa (see later Fig. 5b). One of the
293 conspicuous differences from the figure of Tomita and Yasunari (see their Fig. 1) is the
294 biennial center of SST over the South China Sea. The biennial SST in this area has been
295 stressed by Shen and Lau (1995), and Kawamura (1998), among others. According to these
296 authors, the biennial oscillation in the South China Sea may belong to the Asian monsoon,
297 which is a relatively different phenomenon.

298 A peculiar center of extremely large percentage is found off the Mexican coast in the
299 Pacific (at 13ºN) for both SST and HC fields (Fig. 4). The map of Tomita and Yasunari
300 (1996) (their Fig. 1) also shows a similar center, but a complete explanation of the existence
301 of that maximum of periodicity is missing. In the Indian Ocean, there is a center for SST (max
302 45%), which is located in the South Indian Ocean (east of Madagascar), and that could

303 correspond to the subtropical dipole as discussed by Fauchereau et al. (2003). There is no
304 center of this biennial periodicity in the North Indian Ocean.

305 The quasi-biennial component is clearly found in the HC too (Fig. 4b). The primary center
306 is at western end of the Pacific Ocean for both sides of the equator (max 47.3%). The northern
307 center is located east of Mindanao, *i.e.* 10ºN and 130ºE-150ºE, and the southern center is east
308 of New Guinea, *i.*e. 6ºS, 160ºE-170ºE, though the size of the latter is small. They are the so-
309 called "lobes". There is another center (max, 45%), *i.*e., eastern end of the Pacific Ocean,
310 120º-90ºW. In the Indian Ocean, there is a strong center for HC (max 50%) in the South
311 Indian Ocean. As for the SST case, there is no center in the North Indian Ocean.

312 It can be summarized that the centers of quasi-biennial periodicity are narrower in the HC
313 (Fig. 4b) than those in the SST (Fig. 4a), see for example the 35% contour line. Previous
314 studies have analyzed the biennial character for precipitation (Lau and Sheu, 1988), and for
315 SST (Shen and Lau, 1995 and Tomita and Yasunari, 1996).

316 *4.2 The quasi-biennial mode in El Nino oscillation*

317 Tomita and Yasunari (1996) mentioned that to understand the role of the ENSO/monsoon
318 system in the biennial oscillation it is important to identify the years accordingly. Meehl
319 (1994) explained the TBO phases identifying the role of convective heating anomalies in the
320 Western Pacific altering the atmospheric circulation in winter, thus influencing the evolution
321 and behavior of the subsequent summer monsoon over South Asia.

322 Wright (1985); Ju and Slingo (1995); and Wang et al. (2000) have shown the pattern of
323 atmospheric temperature over the Pacific and Indian Ocean in the cases of non-Type-II cases.
324 The patterns of atmospheric temperature at 1000 mb, for example, are almost symmetrical
325 around the equator, while those at 300 mb are shifted to Northern Hemisphere by 5°. These
326 figures (not shown) illustrate that the patterns over the Pacific are divided into two types. The
327 pattern of temperature at higher levels is of "butterfly type", while that at lower levels is of
328 "horseshoe type" (see Navarra et al., 1999). The butterfly pattern is found in upper

329 tropospheric temperature (e.g. 200 and 300 mb), while the horseshoe pattern is found in the
330 lower tropospheric temperature (e.g. 700, 850 and 1000 mb). The pattern at 500 mb is a
331 mixture of the features for the upper and lower troposphere.
332 In summary, the quasi-biennial periodicity has main centers in correspondence of the La
333 Niña/El Niño oscillation sectors, including the Indian Ocean. Combining results from fig. 3
334 and fig. 4, these centers may be linked with the TBO as well. In the troposphere of MC
335 region, the TBO might be related to another oscillation, the stratospheric quasi-biennial
336 oscillation (QBO), though the association is not strong (for example, Giorgetta et al. 2002;
337 Yamanaka – personal communication). Wright (1968) speculated differences between TBO
338 and QBO, as he wrote that the former "appears not to be directly related to the stratospheric
339 26-month cycle".
340
341 **5. The atmospheric part of the ENSO oscillation**
342 *5.1 The circulation over ENSO region*
343 Despite the complexity of the climatology of wind system in non-ENSO years, the ENSO
344 years show a quite systematic and simple picture, at least in terms of large-scale circulation.
345 ENSO is basically an air-sea coupled system and the Pacific Ocean has a relatively long
346 ocean adjustment timescale. Therefore, a higher degree of predictability can be expected
347 compared to other climate modes. As mentioned in section 4.2, the lower troposphere
348 temperature (T1000) pattern shows simple and systematic structure (i.e., the horseshoe
349 pattern; Wang et al., 2000). Fig. 5b shows the composite of wind anomalies at 1000 mb for El
350 Niño cases based on the ERA40 data. In particular, the anomalies are computed by averaging
351 wind values from 10 El Niño events in the period 1958-2001 (as selected in section 2), in the
352 figure wind anomalies vectors have been masked if not significant at 95% level (fig. 5). The
353 geopotential height patterns are included in fig. 5 as contours (blue (red) colors correspond to
354 negative (positive) values, respectively, and H/L letters evidence positive/negative

355 geopotential height anomalies). During El Nino events, the maximum of wind speed
356 anomalies at 1000 mb level is located at 175ºW, just south of the Equator (fig. 5b).
357 Considering Pacific and Indian sectors, highs of geopotential height are located around 130°E
358 (about over New Guinea in the MC region, slightly south of the Equator). In the lower
359 atmospheric levels, strong north-easterlies anomalies are positioned in the equatorial eastern
360 Indian Ocean (fig. 5b), this pattern is reminiscent of wind anomalies correspondent to a
361 positive IOD (Reverdin and Luyten, 1986; Saji et al., 1999; Webster et al., 1999; Murtugudde
362 et al., 2000).

363 Over latitudes, the circulation extends north and south almost symmetrically within 30ºN-
364 30ºS around the equator in NDJ, while outside of 30ºN-30ºS the activity is stronger in
365 Northern Hemisphere, and the high regularity cannot be guaranteed. At low level, the effect
366 of geography dominates the circulation pattern such as the winds east of Borneo and South
367 China Sea as well as the winds around Australia (fig. 5b).

368 At 200 mb level, the circulation is more symmetrical around the equator and the wind
369 directions are just opposite compared to 1000 mb patterns (Fig. 5). The coherent and
370 systematic picture at 200 mb level (Fig. 5a) is characteristic of upper-atmosphere couplet in
371 both hemispheres. The corresponding temperature field, as previously mentioned, is “the
372 butterfly pattern” (not shown). This feature of circulation was shown earlier by Horel and
373 Wallace (1981) and Arkin (1982) for the global domain. Horel and Wallace (1981) presented
374 a schematic pattern of upper tropospheric circulation, associated with an ENSO event. Arkin
375 (1982) also showed a pair of anticyclonic/cyclonic anomalies straddling the equator during
376 periods of -SOI/+SOI. These pictures are now extended to the Indian Ocean.

377 *5.2 The ENSO oscillation and its time variability*

378 One of the objectives of this section is to show how the effect of ENSO carries the heat to
379 various regions, and to understand what kind of processes is going on, particularly related to
380 ENSO and its variability. SSTA from the HadISST dataset (Rayner et al., 2003) are averaged

381 in the three areas indicated in Fig. 6a, and shown in figs. 6b, 6c, 6d. In these figures SST are
382 used instead of global surface temperature and NDJ means are computed instead of 12-
383 months means as in Hansen et al. (1999). The panel at the bottom (Fig. 6d) shows the time
384 series of SST in NINO3.4. The middle panel (Fig. 6c) shows SST in the extended ENSO
385 region, that corresponds to the tropical (20°S-20°N) Pacific and Indian Oceans. The top panel
386 (Fig. 6b) shows SST in the broadest ocean area between 45ºS-45ºN, thus including both the
387 extended ENSO and NINO3.4 regions.

388 Figs. 6b, 6c and 6d suggest the following. First, in Fig. 6d (NINO3.4 region), the positive
389 peaks correspond to the warm phase (El Niño), and the negative peaks correspond to the cold
390 phase (La Niña) of ENSO. Second, in Fig. 6c (extended-ENSO region), the amplitudes of
391 SST are slightly reduced from those of NINO3.4, but they have the same interannual
392 variability because the SST anomalies are stronger in the central-eastern Pacific than in the
393 western Pacific-Indian sector. The anomalies shown in fig. 6c tend to be negative before
394 1975, but positive after 1976. In the literature it has been shown that the Indian sector
395 experienced a trend in the SST forced by ENSO (Wallace et al., 1998; Saji et al., 1999),
396 moreover in the 1980s and 1990s the ENSO events have been more intense than before.
397 Thirdly, the anomalies shown in Fig. 6b are small, but they have the same interannual
398 variability of the time series shown in figs. 6c and 6d. Actually, they tend to be negative
399 before 1976 and positive just after. Fig. 6b contains the signal of the temperature increase
400 experienced by the Earth in the recent decades and mostly attributed to global warming
401 (Hoerling et al., 2008) and possibly the signal of the climate shift registered in the mid-70s
402 (Miller et al., 1994). If the same analysis is applied to a longer timeserie (e.g. from the end of
403 the 19th century to the present), the trend of the SST averaged in the global ocean between
404 45°S-45°N ("largest domain" in fig. 6) is still evident, while in the other smaller domains it is
405 harder to identify a shift but a decadal timescale variability is detectable. In any case for the
406 purpose of the present study, the focus is on the weight ENSO has on the climate variability.

To link the results from the SST fields to the atmosphere, we have repeated the computations of fig.6 but applied to dry and moist static energy at low levels (fig.7, energy is averaged in all grid points without any masking). Dry static energy is defined as

$$cpT + gz \qquad (1)$$

where cp is the specific heat at constant pressure, T is atmospheric temperature, g is gravity acceleration and z is geopotential height. The moist static energy is the sum of (1) with the moist component Lq, where L is the latent heat and q is specific humidity. For both moist and dry static energy, the peaks in fig. 7c correspond to the peaks in the SST (fig. 6d), and consequently to the warm and cold ENSO phases. The variability of the energy components averaged in the NINO3.4 region agrees with the averages in the other domains. In particular, the correspondence between negative and positive peaks in fig. 7a with the El Nino/La Nina events previously identified, emphasizes the role ENSO plays in the climate variability. Further, even considering the energy values it is possible to recognize a distinction or a change in the variability at timescales longer than one year around the mid-70s, mostly for the extended ENSO region and the area within 45°S-45°N.

The ENSO atmospheric circulation previously described has a crucial role on the way in which the heat, including its moist component, may be spread over wide areas of the Pacific. In fact, fig. 8 shows El Nino and La Nina events composite of vertically integrated moisture component (i.e Lq) of the moist static energy (panels a and b) and of low levels moisture divergence and low levels moisture fluxes (panels c and d). Low levels refer to the vertical integral below 700 mb. During El Nino years, maxima of vertically integrated moisture are localized in the central eastern Pacific Ocean (fig. 8a), while during La Nina positive anomalies exist in the subtropics, with maxima at around 30° both North and South of the equator (fig. 8b). These patterns correspond to the low levels tropospheric moisture divergence (fig. 8c,d; shaded values). In particular, during El Nino events moisture fluxes converge toward the central eastern Pacific (fig. 8c), while during La Nina it diverges from

433 the equator toward the subtropics, northeasterly (southwesterly) in the northern (southern)
434 hemisphere and also to the MC-West Pacific sector (fig. 8d).

435 The above analysis evidences the role of the atmosphere in transporting heat during ENSO
436 events. Other studies mentioned El Nino events might be very effective in transporting heat
437 poleward even through the ocean (Meinen and McPhaden, 2000; Sloyan et al., 2003; Sun,
438 2008; among others). The intensity of the heat transported by the ocean seems to depend on
439 the quantity of heat content stored in the western Pacific (e.g. Sun, 2003). Recently, the
440 observations of more intense central Pacific El Nino events have been related to the SST
441 warming trend of the Pacific warm pool (Lee and McPhaden, 2010).

442 Summarizing this section, the El Niño/La Niña events appear to be a major source of the
443 short-range variation of SST, causing atmospheric convection and transport of heat through
444 the air. In other words, the SST and energy interannual variability is the same in the three
445 regions. The atmospheric circulation system agrees with the transport of heat in
446 correspondence of ENSO events. Besides, the timeseries of SST and energy in the three
447 domains considered evidence a change in the variability before and after 1970s. The feature
448 of varying intensities resemble the time series of the First Principal Component of SST over
449 the equatorial Pacific obtained by Slingo et al. (1999) (their fig. 8), though they use the SST
450 for all months. Concerning the 1976 transition, there must be direct causes (e.g. Santer et al.
451 2003), which are beyond the scope of the present paper.

452

453 **6. Energy and convection in ENSO events**

454 Newell et al. (1972) and Webster (1972) represent pioneer studies of the energetics
455 involved during ENSO. In particular, Webster (1972) points out that “latent heat accounts for
456 nearly all total variance” of energy and “sensible heat is appreciably smaller than latent heat”.
457 More recently, the energetics of ENSO has been studied in terms of conversion of energy to

458 corroborate the delayed oscillator theory (Goddard and Philander, 2000), or in terms of the
459 energy balance between input and storage in the Tropical Pacific (Brown and Fedorov, 2010).
460 Webster and Lukas (1992) justified the plan of TOGA (Tropical Ocean-Global
461 Atmosphere) experiment, which was performed in the Equatorial Pacific east of New Guinea.
462 They mention that "this area represents contribution from latent, radiation, and sensible
463 heating" to the global climate. They show the diabatic heating speculated by an analysis of
464 Hoskins et al. (1989). The amounts of heating were calculated as the residual from the time-
465 averaged thermodynamic equation using the data of ECMWF between 700 and 50 mb for the
466 boreal winter from 1983 to 1989. According to their analysis, maximum heating is positioned
467 just north of the Equator with the NDJ mean dominating the annual value, as for the
468 precipitation pattern (not shown).
469 In the previous section we have described the main features of ENSO in terms of moist and
470 dry static energy, as composite patterns and as time variations. The combination of SST and
471 energy patterns suggests important mechanisms of the El Nino/La Nina oscillation in
472 connection with its circulation. The condensational heat, at least in terms of lower troposphere
473 moisture content and fluxes, released in the case of El Niño is quite different from that of La
474 Niña. In the case of El Niño, it is in the tropical belt between 20ºS-20ºN, and the warm air is
475 advected eastward in the Indian Ocean and the Pacific Ocean. In the case of La Niña, on the
476 other hand, the regions of the largest moisture convergence are displaced to the MC, plus
477 negative divergence anomalies at higher latitudes (fig. 8). Combining the results from figs. 5,
478 6, 7 and 8 it is possible to argue that the ENSO atmospheric wind dynamics is able to explain
479 the distribution and the transport of atmospheric heat from the tropics to the extra-tropics.
480 Due to the lack of precipitation data, an important step toward a global picture of the
481 condensational heat had to wait for satellite measurements. For example, the outgoing
482 longwave radiation (OLR) is indeed a good measure of deep convection, and thus of heating
483 in the Tropics. In particular, the peaks of precipitation tend to occur at the occasions of El

Niño (see for example Arkin and Ardauny, 1989; Janoviak and Arkin, 1991; Xie and Arkin, 1997). However, OLR data are fully available only from the end of 1970s. To have an idea of the global precipitation patterns before 1979, we need to refer to the atmospheric reanalysis, that is the ERA-40 or the NCEP/NCAR, that cover a period longer than the satellite era and match with the time record of our study (i.e. 1958-2001).

6.1 Precipitation datasets in various reanalysis

In this section we use precipitation data from the re-analysis dataset averaged in NDJ. During these months, large amount rainfall areas extend from the MC region to both northeastward and south-eastward (not shown) in correspondence of ITCZ and SPCZ, respectively. Fig. 9 shows NDJ mean precipitation anomalies averaged over eastern Indian and tropical Pacific Ocean (20ºN-20ºS and 80ºE-80ºW) for each year based on a number of reanalysis and datasets. For the ERA-40 reanalysis (see Andersson et al., 2004), the anomalies are mostly negative in the first part of the record, and mostly positive in the last one, with the change around mid 1970s (fig. 9a). A simple relationship between the ENSO events and the amount of precipitation is not easily identifiable.

The precipitation increase from the 1970s may be related to the reports on sudden change in the weather condition and in the unusual warming over the Pacific Ocean (see for example, Douglas et al., 1982, and Nitta and Yamada, 1989). Furthermore, the increase of condensation is more fundamental and closer to the real cause, i.e. the increase of CO_2. As the usage of precipitation data from re-analysis product is questionable because of their reliability on the sparse global rainfall data availability, in the next section we compare the ERA-40 outputs with other available datasets.

Fig. 9 shows NDJ mean precipitation averaged in the tropical Indian-Pacific sector (as in fig. 9) also for other reanalysis products, i.e. JRA-25 (b), NCEP-R-2 (c), GPCP (d) and NCEP/NCAR (e). Except for the NCEP/NCAR dataset, the precipitation values are available only after 1979. In order to compare the amounts of precipitation, a certain reference value is

subtracted equally from the original values of the reanalysis. The reference value that is used here is the NDJ average at 1980. This value is subtracted from monthly values of JRA-25, NCEP-R2, and GPCP. On the other hand, the computation for NCEP/NCAR matches with that applied to ERA-40. The precipitation anomalies with respect to 1980 in GPCP, JRA-25 and NCEP-R2 tend to be positive, even if the values are smaller than for ERA-40 (fig. 9). The number of data assimilated in ERA-40 and NCEP/NCAR re-analyses strongly increased from the end of the 1970s, and this may have artificially affected the mean precipitation.

It is known that large differences exist among various versions of precipitation reanalyis (see Bosilovich et al. 2007). Besides, "the humidity analysis in ERA-40 suffered from several problems, the most important being the definition of the control variable for humidity….related to the Pinatubo eruption in 1991" (Kallberg – personal communication). One of the problems in Q_{lat} of ERA-40 is that the amount of rainfall is overall too large. This is the most serious deficiency of ERA-40, though other aspects of Qlat in ERA-40 are not bad. Avoiding this complication, the ERA-40 dataset is considered as "tentative". A comparison between NCEP/NCAR and ERA-40 precipitation time series (fig. 9d versus fig. 9a) evidences differences between the two datasets. However, even if the amounts are different the precipitation in the tropical Pacific belt tends to increase toward the end of the century and this is confirmed in both datasets.

Adler et al. (2003) and Bosilovich et al. (2007) consider that GPCP is derived entirely from observation, and therefore, GPCP should be a reference. Fig. 10 shows a focus on the equatorial precipitation anomalies (80ºE-280ºE, 5ºN-5ºS) in NDJ for GPCP. Adler et al. (2003) showed a similar plot for NINO3.4 domain. The values of precipitation in each month of NDJ are similar to each other, if they are within the zonal belt of 5ºN-5ºS. But they deviate wildly from each other in the slightly wider belt of, for example, 10ºN-10ºS (not shown). In the 5ºN-5ºS belt maxima correspond to El Niño events.

535 Further conclusions from fig. 10 are as follows. First, the peaks of precipitation are
536 associated with 4 El Niños. In Table A1, there are 5 El Niños after 1959. They are 82/83,
537 86/87, 87/88, 91/92 and 97/98, but the 87/88E is ambiguous in Fig. 10. Second, there are
538 negative peaks, which roughly correspond to La Niña (see Pavlakis et al., 2006), and the
539 minima are lower when averaged near the MC region (not shown). Third, there is a peak at
540 94/95, but its origin is unknown (SST(NDJ) at 94/95 is large). It might be an aborted El Niño.
541 All aspects of the second and third points agree among GPCP, ERA-40, NCEP-R2 and JRA-
542 25. The correlation coefficient between GPCP and ERA-40 is 0.84, that between GPCP and
543 NCEP-R2 is 0.66, and that between GPCP and JRA-25 is 0.54. JRA-25 and NCEP-R2 have a
544 more coherent interannual variability with a correlation coefficient of 0.90.
545 *6.2 Latitudinal distribution of rainfall*
546 Finally, the latitudinal distribution of rainfall is discussed based on the datasets considered.
547 Zonal mean profiles of NDJ mean precipitation are shown in Fig. 11. For ERA-40 and
548 NCEP/NCAR the time mean are separated before and after 1976, while for JRA-25, NCEP-
549 R2 and GPCP the whole available record is used (i.e. 1979-2002).
550 In the ERA-40 the difference in the mean before and after 1976 is limited to the equatorial
551 tropics (between 9ºN-15ºS), with more intense precipitation in the second half of the record
552 (Fig. 11a). This clear difference between and after 1976 is not evident in NCEP/NCAR (fig.
553 11b). The zonal profiles have two peaks with a slight minimum at the equator. The JRA-25
554 assimilation zonal profile (fig. 11c) is closest to that of ERA40, though the peak at 6ºS is
555 weaker. It is a questionable which is more reasonable and possibly correct. According to
556 Kallberg (personal communication), the amount of rainfall that is newly estimated in
557 European Centre would be reduced substantially. Both JRA-25 and ERA40 have values larger
558 than GPCP (fig. 11e). In the extra-tropics, the shapes of curves and the amounts of rainfall
559 are comparable within the datasets.
560

561 **7. Conclusions**

562 Observations and re-analysis datasets have been used to classify ENSO and non-ENSO
563 years to describe typical features of its periodicity and of its spatial patterns. In particular, El
564 Nino and La Nina events have been classified using NINO3 SST and western Pacific upper
565 ocean heat content, respectively. The choice of the heat content and of its average in a specific
566 region (130°-170°E, 2°-10°N, here defined as "north-western lobe") of the western Pacific
567 follows the hypothesis that heat content growth in the western Pacific is precursor to ENSO
568 (Wyrtki, 1975) in the framework of the recharge-discharge oscillator (Jin 1997a, b). The
569 north-western lobe here defined includes just a portion of the western Pacific area involved in
570 the recharge-discharge oscillator paradigm, and to strengthen our choice we have verified that
571 the heat content averaged there is significantly correlated with NINO3 SST. The classification
572 we used mostly agrees with previous studies, and for La Nina cases it may probably be related
573 to oceanic Rossby wave first meridional mode structure that maximizes around 4°-5°S and 4°-
574 5°N.

575 Among non-ENSO years we have identified the so-called type-II years (Navarra et al.,
576 1999) that are characterized by very small anomalies in summer, differently from El Nino and
577 La Nina years and from the equatorial Pacific mean climatology. The existence of these years
578 and their characteristics are important if we consider the relationship between ENSO and
579 tropical precipitation variability. In particular, considering a three-year time window the
580 Indian and Pacific sector have comparable correlation in time and intensities between SST
581 and summer mean TOI, with the MC-Western Pacific sector that represents a sort of transition
582 between them. When the type-II years are excluded from the analysis, the correlation
583 coefficients intensify, thus suggesting a strengthening of that relationship. The longitude
584 extension of the correlation supports the idea of an extended-ENSO region. A frequency
585 analysis of the quasi-biennial periodicity evidence that SST have higher biennial frequency
586 variability along the equator west of NINO3, while the HC has those centers in the western

587 Pacific. In particular, it is possible to identify two lobes, i.e., the northern and southern lobes.
588 The northern center is located east of Mindanao, i.e., 10ºN and 130ºE-150ºE, while the
589 southern center is east of New Guinea, i.e., 6ºS and 160ºE-170ºE. The northern lobe has been
590 used in this study to identify La Niña years.

591 Considering the spatial patterns of the ENSO composites, the systematic picture of the
592 mean circulation in terms of the wind patterns in lower and upper troposphere are described
593 considering an extended-ENSO region that includes also the tropical Indian Ocean.
594 Combining wind and energy patterns, we can conclude that ENSO plays an important role in
595 the release of a large amount of condensational heat in the tropics (20ºN-20ºS) with El Niño,
596 but also on spreading warm air outside the tropics with La Niña. Warming of the tropical
597 troposphere in correspondence with ENSO events is accompanied by an intensified Hadley
598 circulation and associated strengthening of the zonal jet streams in both hemispheres (Yulaeva
599 and Wallace, 1994).

600 Moist and dry static energy, SST and equatorial mean precipitation tend to peak in
601 correspondence of El Nino years. Considering the SST variability, the ENSO signature is
602 evident even when considering larger domains (e.g. global oceans between 45°S-45°N) and
603 on long timescales it is possible to detect a change in its variability around mid 70s. To relate
604 these changes to the precipitation around the equator a specific analysis has been performed
605 using different re-analysis compilations. The datasets available for the whole period of study
606 (i.e. 1958-2001) are ERA40 and NCEP/NCAR. Both are questioned for accuracy (in the case
607 of ERA40, the total amount of heat is questioned but not the relative shape of the rain
608 distribution with latitude), and there is not complete agreement between the two reanalysis,
609 mainly below 700 mb (Hoskins et al., 1989; Nigam et al., 2000). According to ERA-40, the
610 amount of rainfall is much larger after 1976 than that before 1976, particularly in the
611 equatorial tropics. The comparison between ERA40 and other reanalysis products available

612 after 1979 (i.e. GPCP, NCEP-R2 and JRA-25) evidence some agreements, even if a clear
613 conclusion cannot be drawn.

614 The phenomena discussed in this paper are confined to the tropical band (20ºN-20ºS),
615 where the predictability is larger. ENSO is basically an air-sea interaction, relatively slow,
616 steady and systematic. In order to understand the whole structure of ENSO processes, the
617 thermocline of the ocean should also be included. An analysis of the oceanic component of
618 ENSO oscillation will be part of a future work. The cause for the 1976 transition has not been
619 discussed in this paper. It is an interesting question whether this kind of transition may occur
620 again in the future.

621 **Appendix A – Type-II cases**

622 How to select the type-II cases is described in this appendix. As was mentioned in section
623 2, the El Niño and La Niña years are selected by the values of SST at NINO3 and the values
624 of HC in the western lobe, respectively. The remaining years must belong to the type-II or
625 other unidentified cases.

626 Table A1 presents the 43 years data series of El Niño/La Niña events and SST anomalies
627 between La Niña and El Niño in NINO3 (instead of NINO3.4), and HC anomalies in the
628 western lobe of the Pacific Ocean. This table includes four rows of information for each year.
629 The first row is the years, starting at 1959 and ending at 2001. The second row represents the
630 SST anomalies in NINO3 region during NDJ(0), the third row indicates El Niño, La Niña and
631 type-II years, the fourth row indicates SST anomalies in NINO3 region during JAS(0) and
632 finally the fifth row shows the heat content anomalies in the region 130°E-170°E, 2°N-10°N
633 for NDJ(0) (see subsection 2.2). SST and HC used for this table come from the global ocean
634 analysis described by (Masina et al. 2004).

635 Type-II events have been extensively discussed and described in Navarra et al. (1999) and
636 in Miyakoda et al. (1999). In those studies, they have been identified by means of SST and
637 precipitation indices in the Equatorial Pacific. In particular, type-II years are characterized by

small SST anomalies during JAS in the NINO3 region (fig. 2b), and they appear to be crucial for the periodicity of the teleconnection between Asian rainfall and the eastern Pacific (Miyakoda et al., 1999; Navarra et al., 1999). Analyzing JAS NINO3 SSTA in the ocean analysis (Masina et al., 2004) we identified as type-II those years having anomalies less than 0.79°C (corresponding to one standard deviation of the SST variability in that period), thus selecting nine events as shown in Table A1. This selection agrees with results from Navarra et al., 1999 and Miyakoda et al., 1999.

Acknowledgments

We are grateful to the reviewers whose comments helped us to largely improve the manuscript. We express our appreciation to GFDL (Geophysical Fluid Dynamics Laboratory), US Department of Commerce for providing the convenience of the research to K. Miyakoda and J. Ploshay. We are also very much owe to a number of people, particularly Drs. S. Manabe and S.K. Bryan, A.F. Wittenberg, Ms. Cathy Raphael. Dr. P. Kalberg is acknowledged as he provided the unpublished information about the accuracy of ERA-40. The JRA-25 long-term reanalysis cooperative research project carried out by the Japan Meteorological Agency (JMA) and the Central Research Institute of Electric Power Industry (CRIEPI) has been used in this study. We also acknowledge GEMINA project (F.I.S.R. - CIPE n. 42/2010) for financial support.

656 **References**

657 Aceituno P., 1992: El Niño, the Southern Oscillation, and ENSO: Confusing names for a
658 complex ocean-atmosphere interaction. *Bull. Amer. Meteor. Soc.*, **73**, 483-485.

659 Adler R.E., G.J. Huffman, A. Chang, R. Ferraro, P.P. Xie, J. Janoviak, B. Rudolph, U.
660 Schneider, S. Curtis, D. Bolvin, A. Gruber, J. Susskind, P. Arkin, E. Nelkin, 2003: The
661 version-2 global precipitation climatology project (GPCP) monthly precipitation
662 analyses (1979-present). *J. Hydromet.*, **4**, 1147-1167.

663 Andersson E, Bauer P, Beljaars A, Chevallier F, Holm E, Janoskova M, Kalberg P, Kelly G,
664 Lopez P, Mcnally A, Moreau E, Simmons AJ, Thepaut JN, Tompkins AM, 2004:
665 Assimilation and modeling of the atmospheric hydrological cycle in the ECMWF
666 forecasting system. *Bull. Amer. Meteor. Soc.*, **86**, 387-399.

667 Annamalai H, Murtugudde R, Potemra J, Xie SP, Liu P, Wang B, 2003: Coupled dynamics
668 over the Indian Ocean: spring initiation of the zonal mode. *Deep-Sea Res II*, **50**, 2305-
669 2330.

670 Arkin PA, 1982: The relationship between interannual variability in the 200 mb wind field
671 and the Southern Oscillation. *Mon. Wea. Rev.*, **110**, 1393-1404.

672 Arkin PA, Ardanuy PE, 1989: Estimating climate-scale precipitation from space. A review. *J.*
673 *Climate*, **2**, 1229-1238.

674 Ashok K, Behera S, Rao S, Weng H, Yamagata T, 2007: El Nino Modoki and its possible
675 teleconnection. *J Geophys Res*, **112**, C11007, doi: 10.1029/2006JC003798.

676 Barnett TP, 1985: Variations in near global sea level pressure. *J. Atmos. Sci.*, **42**, 478-501.

677 Barnett TP, 1991: The interaction of multiple time scales in the tropical climate system. *J.*
678 *Climate*, **4**, 269-285.

679 Bosc C, Delcroix T, Maes C, 2009: Barrier layer variability in the western Pacific warm pool
680 from 2000 to 2007. *J Geophys Res*, **114**, C06023, doi: 10.1029/2008JC005187.

681 Bosilovich MG, Chen J, Robertson FR, Adler RF, 2007: Evaluation of global precipitation in

682 reanalysis. In: Proceeding. 21st conference on hydrology, San Antonio, Tx.
683 Brown JN, Fedorov AV, 2010: How much energy is transferred from the winds to the
684 thermocline on ENSO time scales? *J. Climate*, **23**, 1563-1580.
685 Chang CP, Li T, 2000: A theory for the Tropospheric Biennial Oscillation. *J Atmos Sci*, **57**,
686 2209-2224.
687 Douglas AV, Cayan DR, Namias J, 1982: Large-scale changes in north Pacific and north
688 American weather patterns in recent decades. *Mon. Wea. Rev.*, **110**, 1857-1862.
689 Fauchereau N, Trzaska S, Richard Y, Roucou P, Camberlin P, 2003: Sea-surface temperature
690 co-variability in the southern Atlantic and Indian oceans and its connections with the
691 atmospheric circulation in the Southern Hemisphere. *Int J Climatol*, **23**, 663-677.
692 Gershunov A, Schneider N, Barnett T (2001) Low-frequency modulation of the ENSO-Indian
693 monsoon rainfall relationship: Signal or noise? *J. Climate*, **14**, 2486-2492.
694 Giorgetta M, Manzini E, Roeckner E, 2002: Forcing of the quasi-bieenial oscillation from a
695 broad spectrum of atmospheric waves. *Geophys. Res. Lett.*, **9**, 861-864.
696 Goddard L, Philander SGH, 2000: The energetics of El Nino and La Nina. *J. Climate*, **13**,
697 1496-1516.
698 Gutzler DS, Harrison DE, 1987: The structure and evolution of seasonal wind anomalies over
699 the near-equatorial eastern Indian and western Pacific Ocean. *Mon. Wea. Rev.*, **151** 169-
700 192.
701 Hansen J, Ruedy R, Glascoe J, Sato M, 1999: GISS analysis of surface temperature change. *J.*
702 *Geophys. Res.*, **104**, No. D24: 30,997-31,022.
703 Harrison DE, Larkin NK, 1998: The ENSO surface temperature and wind signal: a near-
704 global composite and time-series view, 1946-1995. *Rev. Geophys.*, **36**(3): 353-399.
705 Hoerling M, Kumar A, Eischeid J, Jha B, 2008: What is causing the variability in global mean
706 land temperature? *Geophys Res Lett*, **35**, L23712, doi: 10.1029/2008GL035984.
707 Horel JD, Wallace JM, 1981: Planetary scale atmospheric phenomena associated with the

708 Southern Oscillation. *Mon. Wea. Rev.*, **109**: 813-829.
709 Hoskins BJ, Hsu HH, Jawes IN, Matsutani M, Saardeshmukh PD, White GH, 1989:
710 Diagnostics of the global atmosphere circulation based on ECMWF analyses 1979-
711 1989. Tech. Document WCRP-27, WMO/TD-NHo. 326, WMO, 217 pp.
712 Hunt AG, 1999: Understanding a possible correlation between El Nino occurrence frequency
713 and global warming. *Bull. Amer. Meteor. Soc.*, **80**: 297-300.
714 Izumo T, Masson S, Vialard J, de Boyer Montegut C, Behera S, Madec G, Takahashi K,
715 Yamagata T, 2010: Low and high frequency Madden-Julian oscillations in austral
716 summer: interannual variations. *Clim Dyn*, **35**, 669-683.
717 Janowiak JE, Arkin PA, 1991: Rainfall variations in the tropics during 1986-1989, as
718 estimated from observations of cloud-top temperature, *J. Geophys. Res.*, **96**: 3359-3373.
719 Japan Meteorological Agency, 2007: Monthly report on climate system, Separated Volume
720 No. 13, pp 139.
721 Jin FF, 1997a: An Equatorial ocean recharge paradigm for ENSO. Part I: conceptual model. *J*
722 *Atmos Sci*, **54**, 811-829.
723 Jin FF, 1997b: An Equatorial ocean recharge paradigm for ENSO. Part II: A stripped-down
724 coupled model. *J Atmos Sci*, **54**, 830-847.
725 Ju J, Slingo J, 1995: The Asian summer monsoon and ENSO. *Quart. J. Roy. Meteor. Soc.*,
726 **121**, 1133-1168.
727 Kallberg P and Co-authors, 2005: Assimilation and modeling of the atmospheric hydrological
728 cycle in the ECMWF forecasting system. *Bull. Amer. Meteor. Soc.*, **86**, 387-402.
729 Kalnay E and Co-authors, 1996: The NCEP/NCAR 40-year Re-analysis Project. *Bull. Amer.*
730 *Meteor. Soc.,* **77,** 437-471.
731 Kanamitsu M, Ebisuzaki W, Woollen J, Yang SK, Hnilo JJ, Fiorino M, Potter GL, 2002:
732 NCEP-DOE AMIP-II Reanalysis (R-2). *Bull. Amer. Meteor. Soc.*, **83,** 1631-1643.
733 Kao HY, Yu JY, 2009: Contrasting Eastern-Pacific and Central-Pacific types of ENSO. *J*

734 *Climate*, **22**, 615-632.
735 Kawamura R, 1998: A possible mechanism of the Asian summer monsoon-ENSO coupling.
736 *J. Meteor. Soc. Japan*, **76**, 1009-1027.
737 Kessler WS, McPhaden MJ, Weickmann KM, 1995: Forcing of intraseasonal Kelvin waves in
738 the Equatorial Pacific. *J Geophys Res*, **100**, 10 613-10 631
739 Kirtman BP, Shukla J, 2000: Influence of the Indian summer monsoon on ENSO. *Quart. J.*
740 *Roy. Meteor. Soc.*, **126**, 213-239.
741 Kug JS, Jin FF, An SI, 2009: Two types of El Nino events: Cold tongue El Nino and warm
742 pool El Nino. *J Climate*, **22**, 1499-1515.
743 Kumar KK, Rajagopalan B, Cane MA, 1999: On the weakening relationship between the
744 Indian monsoon and ENSO. *Science*, **284**, 2156-2159.
745 Larkin NK, Harrison DE, 2005: Global seasonal temperature and precipitation anomalies
746 during El Nino autumn and winter. *Geophys Res Lett*, **32**, L16705, doi:
747 10.1029/2005GL022860.
748 Larkin NK, Harrison DE, 2002: ENSO Warm (El Nino) and cold (La Nina) Event life cycles:
749 ocean surface anomaly patterns, their symmetries, asymmetries, and implications. *J.*
750 *Climate*, **15**, 1118-1140.
751 Latif M, Kleeman R, Eckert C, 1997: Greenhouse warming, decadal variability, or El Nino?
752 An attempt to understand the anomalous 1990s. *J. Climate*, **10**, 2221-2239.
753 Lau N-C, Nath MJ, 1994: A modeling study of the radiative roles of tropical and
754 extratropical SST anomalies in the variability of the global atmosphere- ocean system.
755 *J. Climate*, **7** ,1184-1207.
756 Lau KM, Sheu P, 1988: Annual cycle QBO and Southern Oscillation in global precipitation
757 in winter. *J. Geophys. Res.*, **93(D9)**, 10975-10988.
758 Lau KM, Yang S, 1996: The Asian monsoon and predictability of the tropical ocean-
759 atmosphere system. *Quart. J. Roy. Meteor. Soc.*, **122**, 945-957.

760 Lee T, McPhaden MJ, 2010: Increasing intensity of El Niño in the central-equatorial Pacific.
761 *Geophys Res Lett*, **37**, L14603, doi:10.1029/2010GL044007.
762 Lengaigne M, Boulanger JP, Menkes C, Spencer H, 2006: Influence of the seasonal cycle on
763 the termination of El Nino events in a coupled general circulation model. *J. Climate*, **19**,
764 1850-1868.
765 Maes C, Sudre J, Garcon V, 2010: Detection of the eastern edge of the equatorial Pacific
766 warm pool using satellite-based ocean color observations. *SOLA*, **6**, 129-132.
767 Masina S, Di Pietro P, Navarra A, 2004: Interannual-to-decadal variability of The North
768 Atlantic from an ocean data assimilation system. *Clim. Dyn.*, **23**, 531-546.
769 McPhaden MJ, Zhang X, 2009: Asymmetry in zonal phase propagation of ENSO sea surface
770 temperature anomalies. *Geophys Res Lett*, **36**, L13703, doi:10.1029/2009GL038774.
771 Meehl GA, 1987: The annual cycle and interannual variability in the tropical Pacific and
772 Indian Ocean regions. *Mon. Wea. Rev.*, **115**, 27-50.
773 Meehl GA, 1994: Coupled land-ocean-atmosphere processes and South Asian monsoon
774 variability. *Science*, **266**, 263-267.
775 Meehl GA, 1997: The South Asian monsoon and the tropospheric biennial oscillation. *J.*
776 *Climate*, **10**, 1921-1943.
777 Meinen CS, McPhaden MJ, 2000: Observations of Warm Water Volume Changes in the
778 Equatorial Pacific and Their Relationship to El Nino and La Nina. *J Climate*, **13**, 3551-
779 3559.
780 Miller AJ, Cayan DR, Barnett TP, Graham NE, Oberhuber JM, 1994: The 1976-77 climate
781 shift of the Pacific Ocean. *Oceanography*, **7**, 20-26.
782 Miyakoda K, Kinter JL, Yang S, 2000: Analysis of the connection from the South Asian
783 monsoons to ENSO by using precipitation and circulation indices. COLA Tech. Rep.,
784 90, 72p.
785 Miyakoda K, Navarra A, Ward MN, 1999: Tropical-wide teleconnection and oscillation. II:

786 The ENSO-monsoon system. *Quart J Roy Meteorol Soc*, **125**, 2937-2963.
787 Murakami M, 1979: Large-scale aspects of deep convective activity over the GATE area.
788 *Mon. Wea. Rev.,* **107**, 994-1013.
789 Murtugudde R, McCreary JP, Busalacchi AJ, 2000: Oceanic processes associated with
790 anomalous events in the Indian Ocean with relevance to 1997-1998. *J Geophys Res*,
791 **105(C2)**, 3295-3306.
792 Navarra A, Ward MN, Miyakoda K, 1999: Tropical-wide teleconnection and oscillation. I.
793 Teleconnection indices and type I/type II states. *Quart. J. Roy. Meteor. Soc.*, **125**,
794 2909-2936.
795 Neelin JD, Jin FF, Syu HH, 2000: Variations in ENSO phase locking. *J. Climate*, **13**, 2570-
796 2590.
797 Newell RE, Kidson JW, Vincent DG, Boer GJ, 1972: The general circulation of the tropical
798 atmosphere and interaction with extratropical latitudes. The MIT Press, pp. 258-371.
799 Nigam S, Chung C, and Weaver ED, 2000: ENSO diabatic heating in ECMWF and NCEP-
800 NCAR Reanalysis, and NCAR CCM3 simulation. *J. Climate*, **13**, 3152-3171.
801 Nitta T, Yamada S, 1989: Recent warming of tropical sea surface temperature and its
802 relationship to the Northern hemisphere circulation. *J. Meteor. Soc. Japan*, **67**, 375-383.
803 Palmer T, Mansfield DA, 1984: Response of two atmospheric general circulation models to
804 sea-surface temperature anomalies in the tropical East and West Pacific. *Nature*, **310**,
805 483-485.
806 Pavlakis KG and Co-authors, 2006: ENSO surface longwave radiation forcing over the
807 tropical Pacific. *Atmos. Chem. Phys. Discuss*, **6**, 12895-12928.
808 Picaut J, Ioualalen M, Menkes C, Delcroix T, McPhaden MJ, 1996: Mechanism of the zonal
809 displacements of the Pacific warm pool: Implications for ENSO. *Science*, **274**, 1486-
810 1489.
811 Pillai PA, Mohankumar K, 2008: Local Hadley circulation over the Asian monsoon region

associated with the Tropospheric Biennial Oscillation. *Theor. Appl. Climatol.*, **91**, 171-179.

Rasmusson EM, Carpenter TH, 1982: Variations in tropical sea surface temperature and surface wind fields associated with the Southern Oscillation/El Niño. *Mon Wea Rev*, **110**, 354-384.

Rasmusson EM, Carpenter TH, 1983: The relationship between eastern equatorial Pacific sea surface temperature and rainfall over India and Sri Lanka. *Mon. Wea. Rev.*, **111**, 517-528.

Rayner NA and co-authors, 2003: Global analysis of sea surface temperature, sea-ice and night marine air temperature since the late nineteenth century. *J Geophys Res*, **18**, 4407, doi: 10.129/2002JD002670.

Reverdin G, Luyten J (1986) Near-surface meanders in the Equatorial Indian Ocean. *J. Phys. Oceanogr.,* **16**, 1088-1100.

Ropelewski CF, Halpert MS, 1996: Quantifying Southern Oscillation- precipitation relationship. *J. Climate*, **9**, 1043-1059.

Saji NH, Goswami BN, Vinaychandran PN, Yamagata T, 1999: A dipole mode in the Tropical Indian Ocean. *Nature*, **401**, 360–363.

Santer BD and Co-authors, 2003: Contributions of anthropogenic and natural forcing to recent tropopause height changes. *Science*, **301**, 479-483.

Schneider U, Fleer HE, 1989: Development of sea surface temperature, surface wind and divergence anomalies during a composite ENSO episode. *Theor. Appl. Climat.*, **39**: 146-159.

Shen S, Lau KM, 1995: Biennial oscillation associated with the east Asian monsoon and tropical sea surface temperature. *J. Meteor. Soc. Japan*, **73**, 105-124.

Shukla J, 1995: Predictability of the tropical atmosphere, the tropical oceans and TOGA. In: Proc. Internat. Conference on Tropical Ocean Global Atmosphere (TOGA) Programme,

838 Vol. 2, WCRP., 91pp. 725-750. World Climate Research Programme, Geneva,
839 Switzerland.
840 Simmons AJ, Gibson JK, 2000: The ERA-40 project plan. ERA-20 Project Report Series 1.
841 ECMWF, Reading, U.K., 62 pp.
842 Slingo J, Rowell DP, Sperber K, Nortley F 1999: On the predictability of the interannual
843 behaviour of the Madden-Julian Oscillation and its relationship with El Nino. *Quart. J.*
844 *Roy. Meteor. Soc.*, **125**, 583-609.
845 Sloyan BM, Johnson GC, Kessler WS, 2003: The Pacific Cold Tongue: A Pathway for
846 Interhemispheric Exchange. *J Phys Oceanogr*, **33**, 1027-1043.
847 Sun DZ, 2008: The role of El Nino – Southern Oscillation in regulating its background state.
848 In: Nonlinear Dynamics in Geosciences, Eds. J. Elsner and A. Tsonis, p. 537-555.
849 Sun DZ, 2003: A Possible Effect of an Increase in the Warm-Pool SST on the Magnitude of
850 El Nino Warming. *J Climate*, **16**, 185-205.
851 Tomita T, Yasunari T, 1996: Role of the northeast winter monsoon on the biennial oscillation
852 of the ENSO/monsoon system. *J. Meteor. Soc. Japan*, **74**, 399-413.
853 Trenberth KE, 1975: A quasi-biennial standing wave in the Southern Hemisphere
854 interrelations with sea surface temperature. *Quart. J. Roy. Meteor. Soc.*, **101**, 55-74.
855 Trenberth KE, 1997: The definition of El Nino. *Bull. Amer. Meteor. Soc.*, **78**, 2771- 2777.
856 Uppala SM and co-authors, 2005: The ERA-40 reanalysis. *Quart. J. Roy. Meteor. Soc.*, **131**,
857 2961-3012.
858 Vecchi GA, Harrison DE, 2003: On the termination of the 2002-3 El Niño event. *Geophys*
859 *Res. Lett.*, **30(18)**, 1964-1967.
860 Wallace JM, Rasmusson EM, Mitchell TP, Kousky VE, Sarachik ES, von Storch H, 1998: On
861 the structure and evolution of ENSO-related climate variability in the tropical Pacific:
862 Lessons. *J. Geophys. Res.*, **103 (C7)**, 14 241–14 260.
863 Wang B, Wu R, Fu X, 2000: Pacific-East Asian teleconnection: How does ENSO affect East

Asian climate? *J. Climate*, **13**, 1517-1536.

Wang C, 2001: A unified oscillator model for the El Nino – Southern oscillation. *J. Climate*, **14**, 98-115.

Webster P, 1972: Response of the tropical atmosphere to local steady forcing. *Mon. Wea. Rev.*, **100**, 518-541

Webster PJ, Lukas R, 1992: TOGA COARE: The coupled ocean-atmosphere response experiment. *Bull. Amer. Meteor. Soc.*, **73**, 1377-1416.

Webster PJ, Moore AM, Loschnigg JP, Leben RR, 1999: Coupled ocean-atmosphere dynamics in the Indian Ocean during 1997-1998. *Nature*, **401**, 356-360.

Webster PJ, Yang S, 1992: Monsoon and ENSO: Selectively interactive system. *Quart. J. Roy. Meteor. Soc.*, **80**, 629-638.

Wright PB, 1968: A widespread biennial oscillation in the troposphere. *Weather*, **23**, 50-54.

Wright PB, 1985: The Southern Oscillation: An ocean-atmosphere feedback System? *Bull. Amer. Meteor. Soc.*, **65**, 398-412.

Wyrtki K, 1975: Fluctuations of the dynamic topography in the Pacific Ocean. *J Phys Oceanogr*, **5**, 450-459.

Xie P, Arkin PA, 1997: An intercomparison of gauge observations and satellite estimates of monthly precipitation. *J. Appl. Meteor.*, **34**, 1143-1160.

Yang SC and co-authors, 2006: ENSO bred vectors in coupled ocean-atmosphere general circulation models. *J. Climate*, **19**, 1422-1436.

Yasunari T, 1985: Zonally propagating modes of the global east-west circulation associated with the Southern Oscillation. *J. Meteor. Soc. Japan*, **63**, 1013-1029.

Yasunari T, 1990: Impact of Indian monsoon on the coupled atmosphere/ocean system in the tropical Pacific. *Meteor. Atmos. Phys.*, **44**, 29-41.

Yeh SW, Kug JS, Dewitte B, Kwon MH, Kirtman B, Jin FF, 2009: El Nino in a changing climate. *Nature*, **461**, 511-514.

890 Yulaeva E, Wallace JM, 1994: The signature of ENSO in global temperature and precipitation
891 fields derived from the Microwave Sounding Unit. *J Climate*, **7**, 1719-1736.
892

892 **Tables**

893

Classification of La Nina events	Trenberth (1997)	Ropelewski and Halpert (1996)	Harrison and Larkin (1998)
In common	64/65, 73/74, 75/76, 88/89, 95/96	67/68, 70/71, 73/74, 75/76, 88/89	64/65, 70/71, 73/74, 75/76, 88/89, 95/96
extra	84/85	71/72	
missing	67/68	64/65, 95/96	67/68

894

895 **Table 1**: Comparison of the classification of La Nina events used in the present study with
896 some previous works, i.e. Trenberth (1997), Ropelewski and Halpert (1996) and Harrison and
897 Larkin (1998). For each study, common, extra and missing cases compared to our
898 classification are indicated in second, third and fourth row, respectively.

899

	1958	1959	1960	1961	1962	1963	1964	1965	1966	1967	1968
SST(NDJ)	-0.61	-0.66	-1.00	-0.94	-1.01	0.57	-1.32	1.01	-0.97	-1.29	0.16
E/L, II		II				E	L	E		L	E
SST(JAS)	-0.50	-0.71	-1.42	-1.23	-1.28	0.17	-1.71	0.86	-0.79	-1.20	-0.51
HC (NDJ)	-0.97	-1.27	-0.22	0.32	0.83	-0.84	0.62	-1.85	0.37	0.41	-0.05

	1969	1970	1971	1972	1973	1974	1975	1976	1977	1978	1979
SST(NDJ)	0.53	-1.71	-1.12	2.13	-1.90	-0.68	-1.32	1.07	0.31	0.01	1.31
E/L, II	II	L		E	L		L	E	II	II	
SST(JAS)	-0.16	-2.00	-0.91	1.48	-1.85	-0.57	-0.89	1.38	0.02	-0.61	1.24
HC(NDJ)	-0.47	0.91	0.89	-1.72	1.40	0.91	1.43	-0.82	-0.22	0.54	0.03

	1980	1981	1982	1983	1984	1985	1986	1987	1988	1989	1990
SST(NDJ)	-0.27	-0.18	3.07	-0.24	-0.47	-0.32	1.06	0.89	-1.39	-0.24	0.20
E/L, II	II		E			II	E	E	L	II	
SST(JAS)	0.01	-0.37	1.59	1.97	-0.45	-0.07	0.58	1.37	-1.55	0.09	0.59
HC(NDJ)	0.03	1.00	-1.53	-0.12	0.79	0.32	-1.02	-1.28	1.60	0.30	-0.81

	1991	1992	1993	1994	1995	1996	1997	1998	1999	2000
SST(NDJ)	1.49	0.26	0.83	1.04	-0.55	-0.46	3.73	0.23	-1.42	-0.40
E/L, II	E				L	II	E		L	II
SST(JAS)	1.17	0.34	0.92	0.31	0.05	0.11	3.29	1.19	-0.54	0.10
HC(NDJ)	-1.51	-0.62	-0.91	-0.99	0.79	1.11	-2.21	1.32	1.77	1.60

Table A1. Classification of El Niño, La Niña, and type-II years for the period 1959-2001 (SST and HC data are taken from the ocean re-analysis by Masina et al., 2004). SST anomalies are averaged in the NINO3 region, while HC anomalies are averaged in the region 130ºE-170ºE, 2ºN-10ºN. JAS refers to the year indicated in the 1st row, while NDJ includes ND of the year specified, and J of the year after.

Figure captions

Figure 1: NDJ mean SST anomalies (°C) averaged between 4^0N-4^0S for some (a) type-I-west years (La Niña, i.e. 1973/74, 1988/89, 1995/96), (b) type-I-east years (El Niño, i.e. 1972/73, 1986/87, 1991/92), and (c) type-II years (i.e. 1978/79, 1985/86, 1989/90) taken from Table A1. Anomalies are computed with respect to 1958-2001 mean climatology using HadISST dataset.

Figure 2: Seasonal SSTA averaged in the NINO3 region for (a) some years from 1958 to 2001, including El Nino, La Nina and non-ENSO events (as specified in the legend); and for (b) the type-II cases classified from Table B1.

Figure 3: (a) "The 3-year correlation diagram" (longitude-time diagram) of lag correlation between TOI in JAS and monthly SST anomalies averaged in the 10^0N-10^0S belt along the Indo-Pacific region. The ordinate is the lead/lag time from Jan(-1) (top) to Dec(+1) (bottom). Values lower (larger) than –0.4 (0.4) are shaded. (b) is the same as (a) but type-II years (defined in Table A1) are excluded. Note that orange (blue) is used for negative (positive) correlations.

Figure 4: Ratio (%) of the biennial component (18-36 months band-pass filter) over the total of (a) SST and (b) HC normalized monthly mean anomalies.

Figure 5: El Niño composites of wind (m/s) directions (vector) and magnitude (shaded), and of geopotential height (m, as contours) anomalies at (a) 200 mb and (b) 1000 mb. Positive (negative) geopotential height anomalies are red (blue), and high/low centers (H/L) are evidenced. Wind vectors and magnitude are masked if not significant at 95% level.

Figure 6: (a) Scheme of the three domains used for the average of SST in the left panels: NINO3.4 (orange box), extended-ENSO (blue-contoured box) and largest domain (bounded by solid black lines). (b) NDJ mean SSTA averaged over the largest domain (ocean points bounded by the solid lines at about 45°N and 45°S). (c) NDJ mean SSTA averaged over the extended-ENSO region (ocean points within blue-contoured area), and (d) NDJ mean SSTA

935 over NINO3.4 region (orange box).

936 **Figure 7:** NDJ mean anomalies of dry and moist static energy (10^2 m^2/s^2) at 1000 mb
937 averaged (a) between 45°S-45°N, (b) in the extended-ENSO region and (c) in the NINO3.4
938 region. The energy values have been computed from NCEP/NCAR reanalysis fields.

939 **Figure 8:** Composite of NDJ (a,b) vertically integrated moist static energy minus dry static
940 energy (i.e. Lq) anomalies (10^6 m^2/s^2) and (c,d) low levels moisture divergence ($kgm^{-2}day^{-1}$,
941 shaded) and low levels moisture fluxes ($kgm^{-1}s^{-1}$, vectors) for El Nino (upper panels) and La
942 Nina (lower panels) years, respectively. Low levels field are integrated in the lower
943 troposphere, below 700 mb.

944 **Figure 9:** NDJ mean precipitation anomalies (mm/day) averaged in the tropical central
945 eastern Pacific of 20^0S-20^0N and 80^0E-280^0E based on (a) ERA-40, (b) JRA-25, (c) NCEP-
946 R2, (d) GPCP and (e) NCEP/NCAR reanalysis.

947 **Figure 10:** NDJ mean precipitation anomalies (mm/day) averaged in the domain 80^0-280^0E,
948 5^0S-5^0N from GPCP.

949 **Figure 11**: Zonal mean NDJ precipitation (mm/day) for (a) ERA40 (before and after 1976),
950 (b) NCEP/NCAR (before and after 1976), (c) JRA-25, (d) NCEP-R2 and (e) GPCP datasets.

951

951 **FIGURE 1**

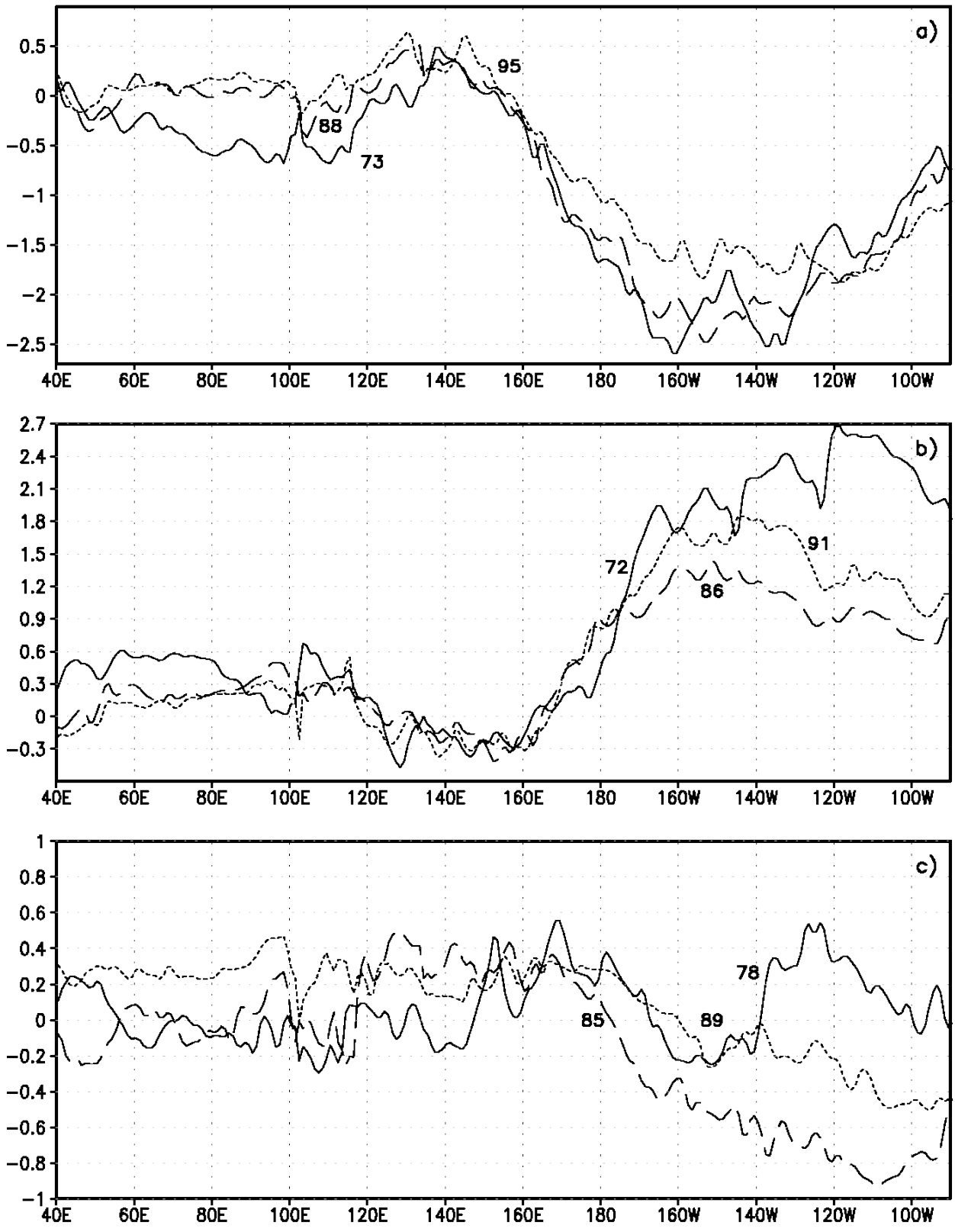

952

953

953 **FIGURE 2**

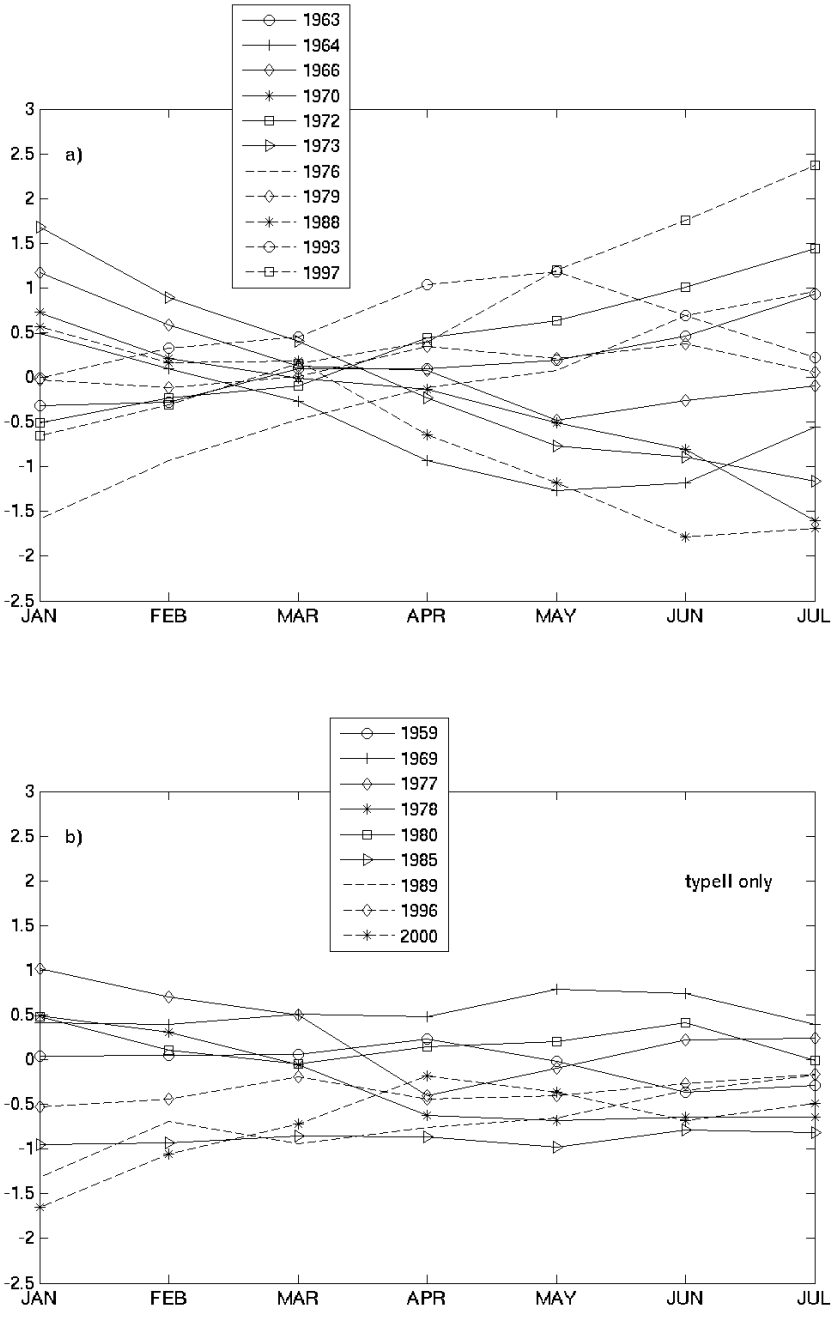

954

FIGURE 3

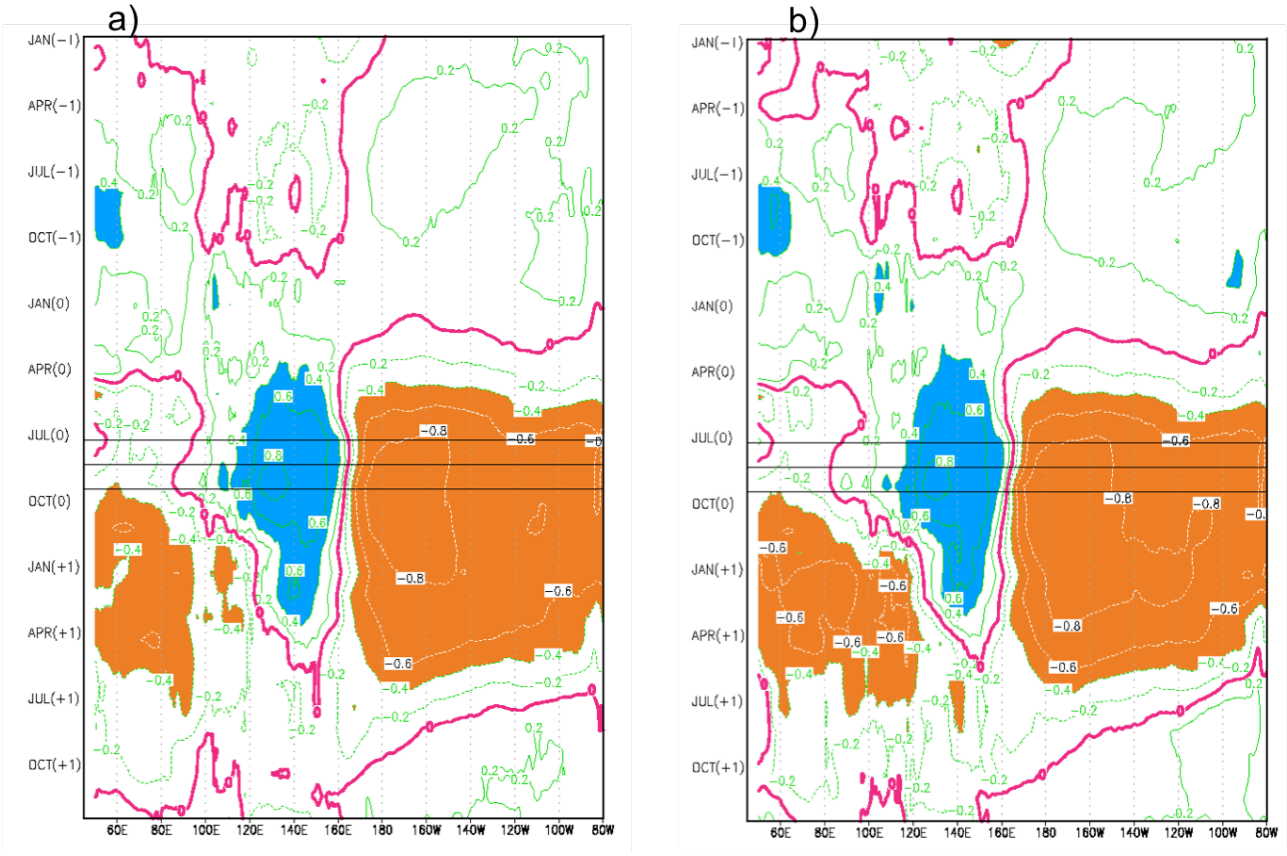
a)
b)
JAN(−1)
APR(−1)
JUL(−1)
OCT(−1)
JAN(0)
APR(0)
JUL(0)
OCT(0)
JAN(+1)
APR(+1)
JUL(+1)
OCT(+1)
60E
80E
100E
120E
140E
160E
180
160W
140W
120W
100W
80W

FIGURE 4

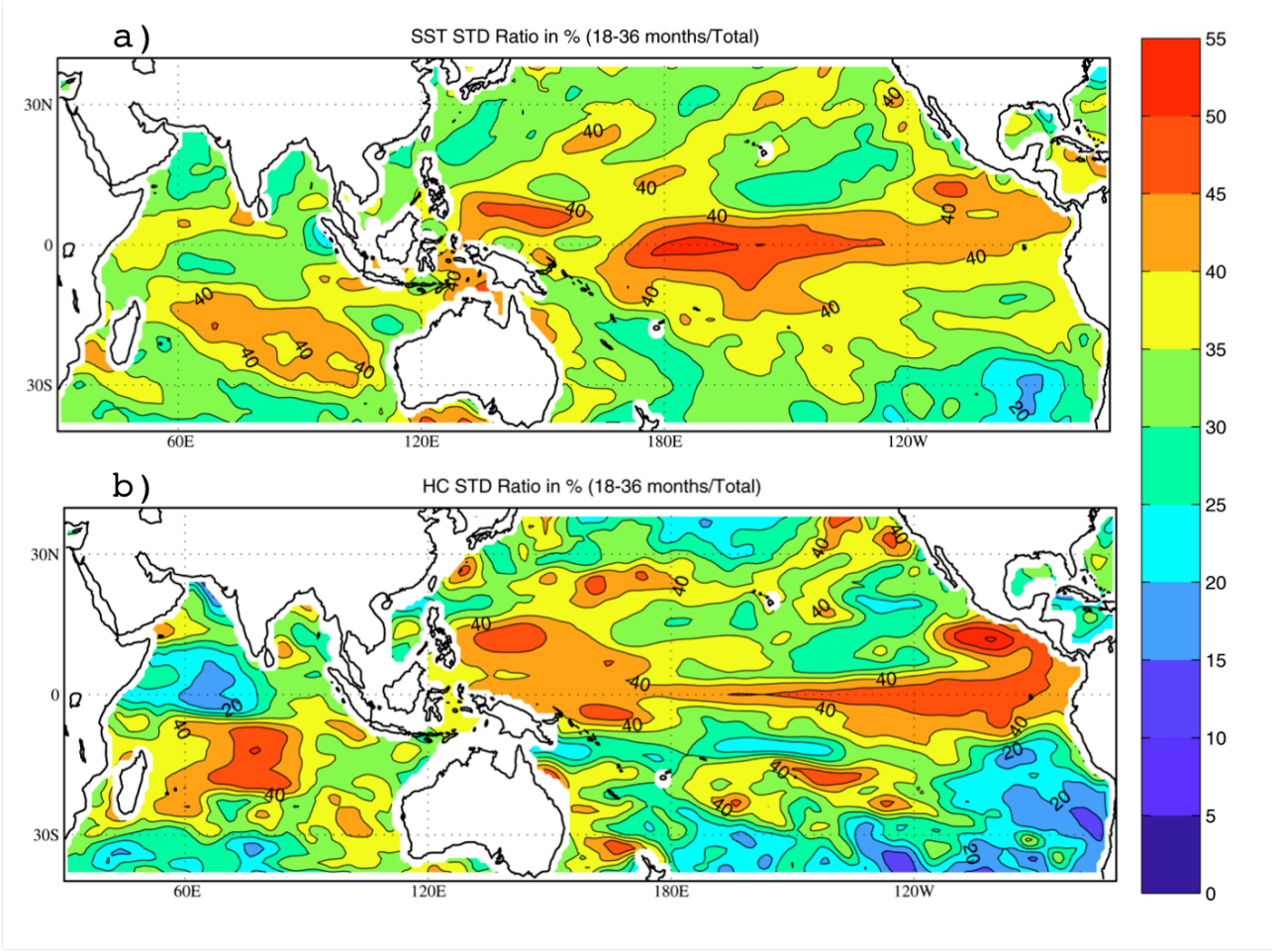
a)
SST STD Ratio in % (18-36 months/Total)
30N
0
30S
60E
120E
180E
120W
b)
HC STD Ratio in % (18-36 months/Total)
30N
0
30S
60E
120E
180E
120W
55
50
45
40
35
30
25
20
15
10
5
0

960 **FIGURE 5**

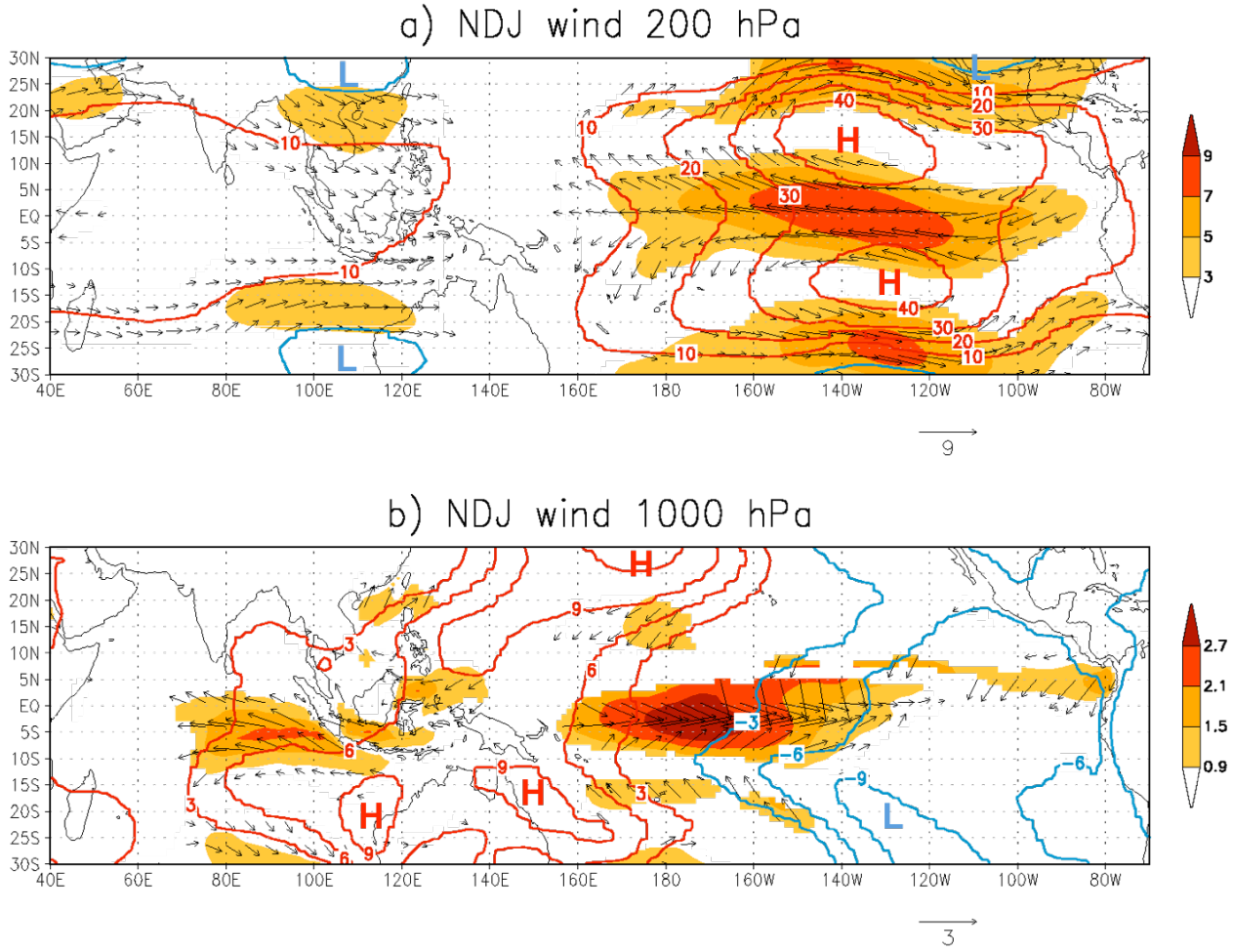

961

962

962 **FIGURE 6**

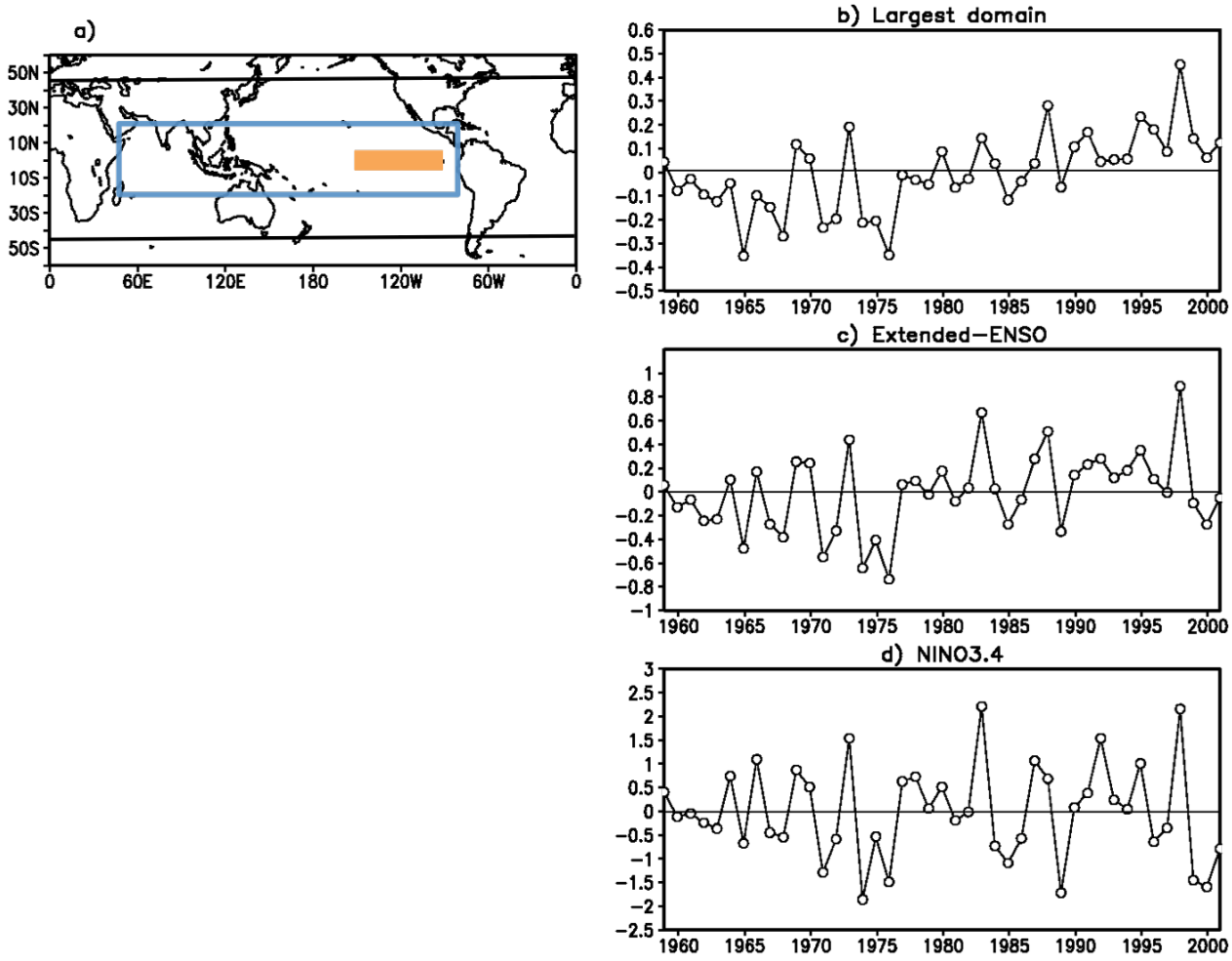

963

964

964 **FIGURE 7**

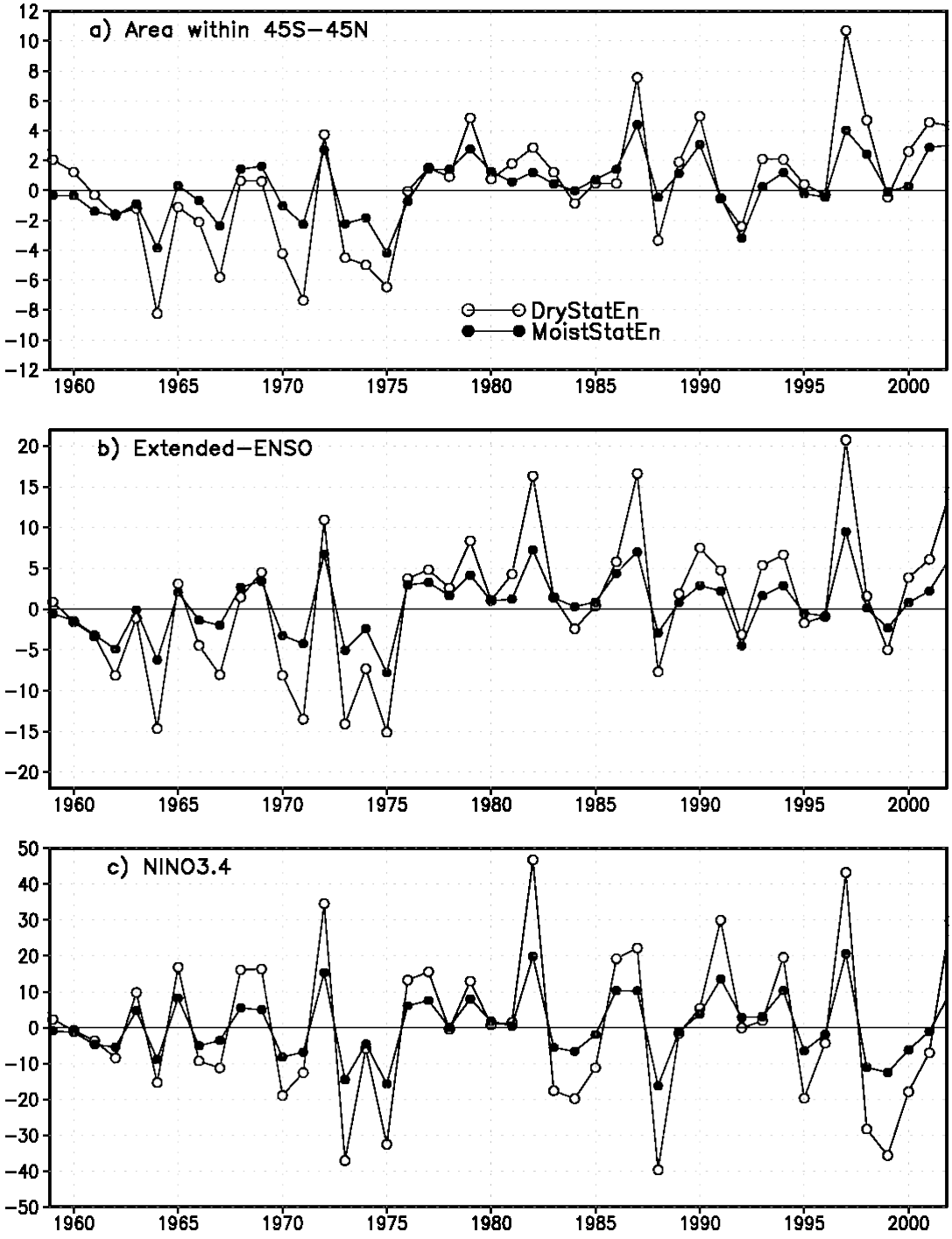

965

966

967

967 **FIGURE 8**

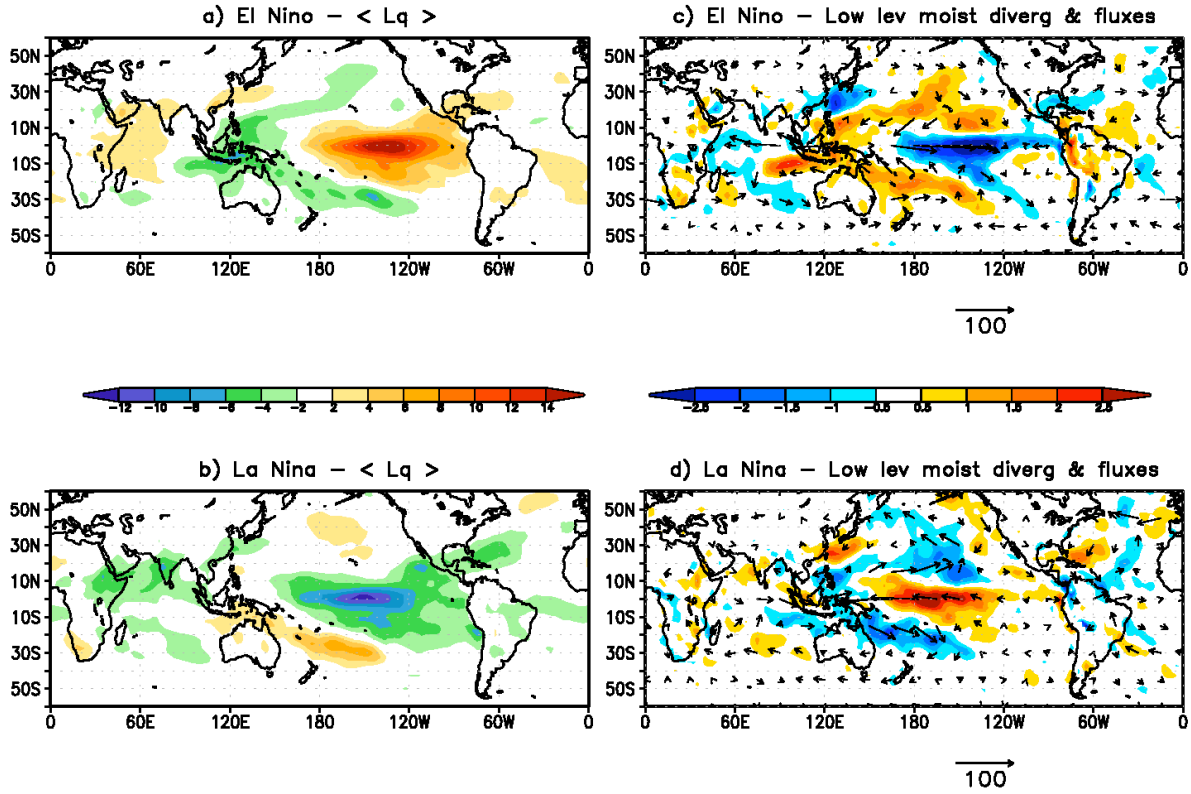

968

969 **FIGURE 9**

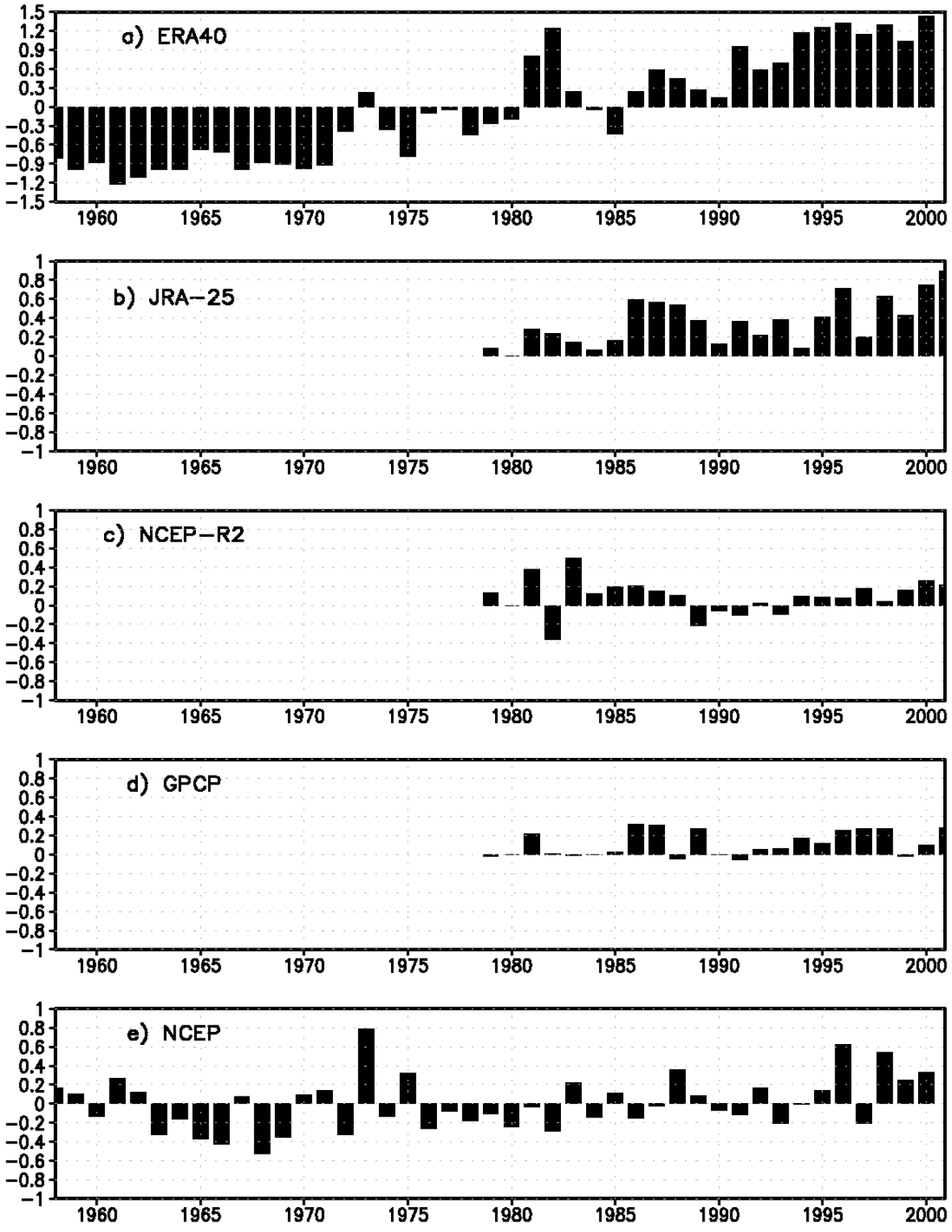

970

971

971 **FIGURE 10**

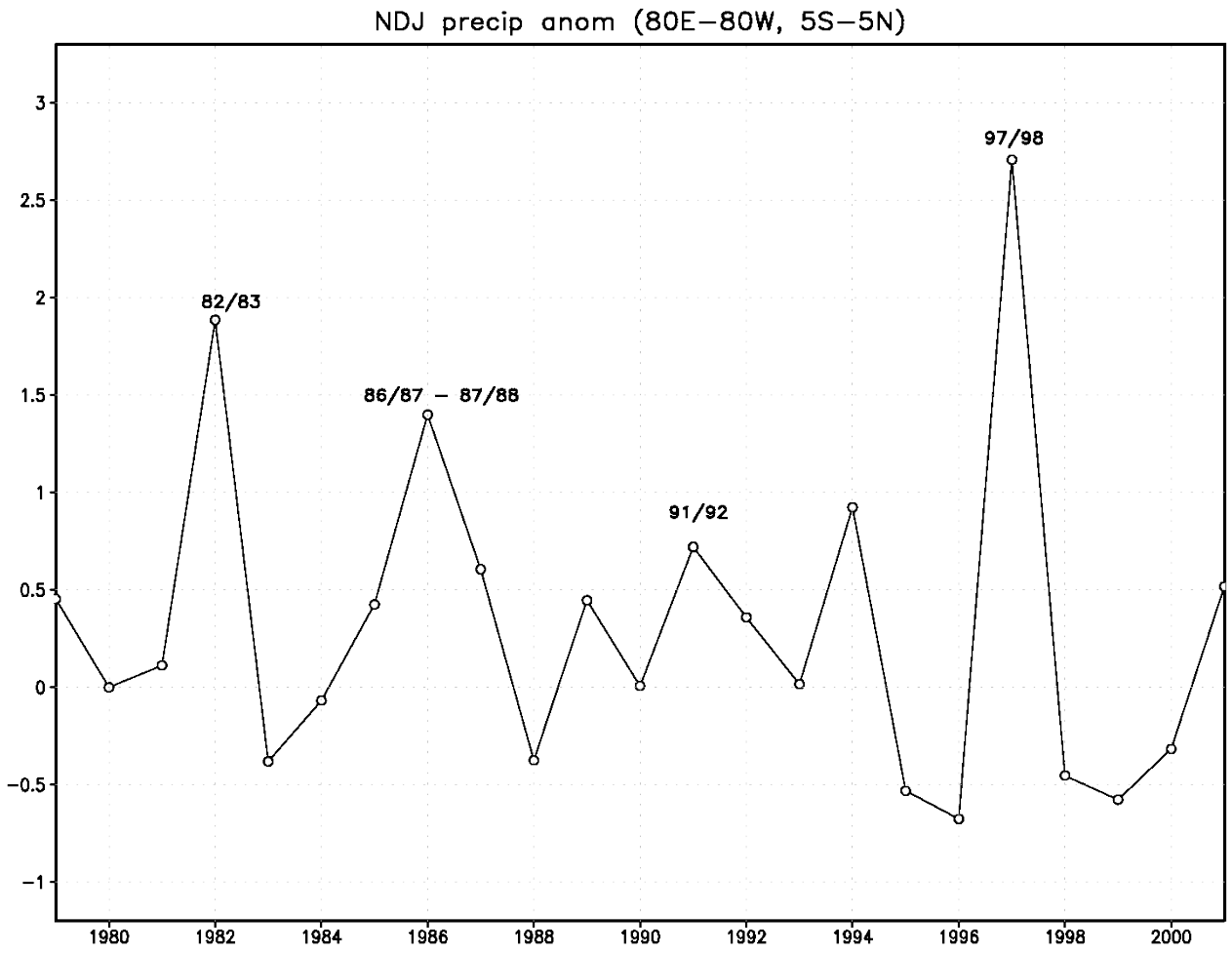

972

973

974

974 **FIGURE 11**

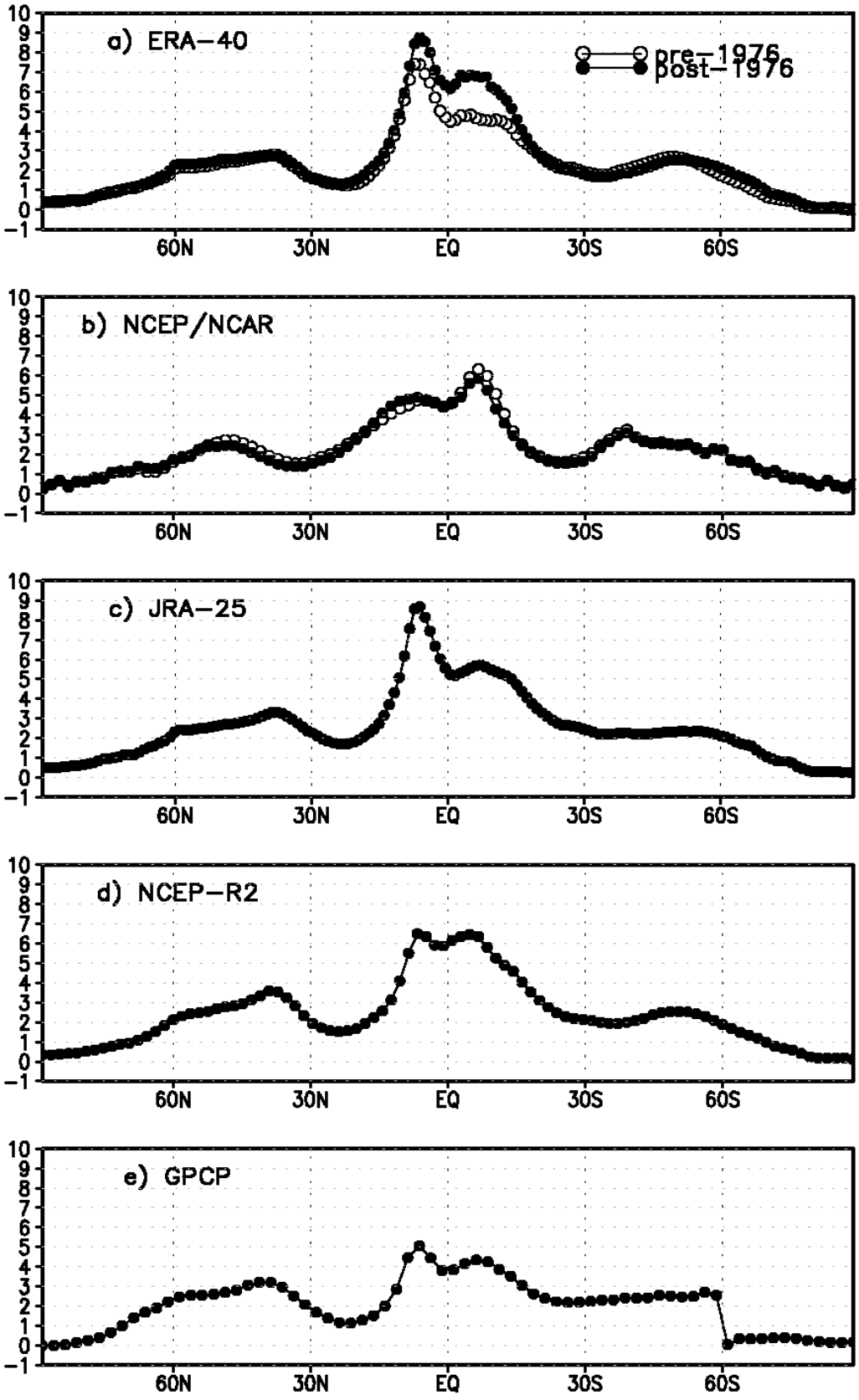

975